UAB
Universitat Autònoma de Barcelona

Dipòsit digital de documents de la UAB

This is the **submitted version** of the journal article:

DeSilva, Jeremy M. [et al.]. «New hominin postcranial fossils from Kromdraai, South Africa (2014–2025)». *Anatomical Record*, August 2026 DOI doi: 10.1002/ar.70300

This version is available at https://ddd.uab.cat/record/337919

under the terms of the IN COPYRIGHT license.

Submission to: Anatomical Record

New hominin postcranial fossils from Kromdraai, South Africa (2014-2025)

- Jeremy M. DeSilva, Department of Anthropology, Dartmouth College, Hanover, NH, USA; Evolutionary Studies Institute, University of the Witwatersrand, Johannesburg, South Africa. jeremy.m.desilva@dartmouth.edu
- Catherine K. Miller, Biomedical Sciences Department, Grand Valley State University, Allendale, MI, USA. millec1@gvsu.edu
- Marine Cazenave, Max Planck Institute for Evolutionary Anthropology, Leipzig, Germany. marine_cazenave@eva.mpg.de
- Gideon Chinamatira, School of Physics, University of the Witwatersrand, Johannesburg, South Africa. gideonchinamatira@gmail.com
- Habiba Chirchir, Department of Anthropology, The Ohio State University, Columbus, OH, USA. chirchir.4@osu.edu
- Ashley S. Hammond, Institut Català de Paleontologia Miquel Crusafont (ICP), Sabadell, Spain. Institució Catalana de Recerca I Estudis Avançats (ICREA), Barcelona, Spain. Division of Anthropology, American Museum of Natural History, New York, NY, USA. ashley.hammond@icp.cat
- Tracy L. Kivell, Max Planck Institute for Evolutionary Anthropology, Leipzig, Germany. Evolutionary Studies Institute, University of the Witwatersrand, Johannesburg, South Africa. tracy_kivell@eva.mpg.de
- Klara Komza, Department of Anthropology, Dartmouth College, Hanover, NH, USA. Klara.Komza@dartmouth.edu
- Ellison J. McNutt, Department of Biomedical Sciences, Colorado State University School of Medicine, Aurora, CO, USA. Ellie.McNutt@colostate.edu
- Kimberleigh Tommy, Evolutionary Studies Institute, University of the Witwatersrand, Johannesburg, South Africa. National Geographic Society. kimberleightommy@gmail.com
- John F. Thackeray, Evolutionary Studies Institute, University of the Witwatersrand, Johannesburg, South Africa. mrsples@global.co.za
- Zewdi Tsegai, Department of Organismal Biology and Anatomy, University of Chicago, Chicago, IL, USA. ztsegai@uchicago.edu
- Alessandra Vecino Gazabón, Division of Anthropology, American Museum of Natural History, New York, NY, USA. avecinogazabon@amnh.org
- José Braga, Center for Anthropobiology and Genomics of Toulouse, Université of Toulouse. jose.braga@univ-tlse3.fr
- Bernhard Zipfel, Evolutionary Studies Institute, University of the Witwatersrand, Johannesburg, South Africa. Bernhard.Zipfel@wits.ac.za

Abstract

Kromdraai, South Africa is the type locality of *Paranthropus robustus*. Renewed paleontological exploration of the site has yielded over 50 hominin fossils since 2014, including 21 postcranial elements. These finds nearly triple the number of postcranial remains previously known from Kromdraai. We describe here four partial humeri, five manual phalanges, two femora, two patellae, and eight pedal elements. Twenty of the fossils derive from Unit P, which dates to over 2.0 million years old and includes craniodental material from *Paranthropus* and *Homo*. One fossil, a patella, may derive from the stratigraphically older Unit O. Interestingly, while more than half of the craniodental remains from Unit P are identified as juvenile, all of the postcrania are adult. Furthermore, though none of the postcrania are directly associated with craniodental finds, we tentatively propose taxonomic assignments for some of these fossils, including two humeri and two femora that may belong to *Paranthropus*.

Keywords: Kromdraai, fossil, hominin, postcrania, South Africa, cradle of humankind, early Pleistocene

Introduction

Kromdraai (26°00’41”S, 27°44’60”E, altitude 1470m; Figure 1) is a fossiliferous, unroofed dolomitic cave chamber located within the UNESCO World Heritage Site known as the “Cradle of Humankind.” It is located on the south side of the Blauuwbank River (Gauteng Province, South Africa), just east of the hominin-bearing cave localities of Swartkrans, Sterkfontein, and Cooper’s. David Draper discovered micromammal fossils on the Kromdraai farm in 1895 and sent samples of cave breccia to the British Museum of Natural History (Draper, 1896; de Graaf, 1961; Malan, 1959). The precise provenance of these early finds is uncertain and cannot be securely tied to the exposures that define the currently recognized Kromdraai site.

The first hominin fossils from Kromdraai were not identified until 1938, when Robert Broom– assisted by local schoolboy Gert Terblanche– discovered ex situ a partial cranium and dentition, believed to be associated with several postcranial elements, and regarded at the time as a supposedly single individual catalogued as TM 1517. Broom subsequently designated this specimen as the holotype of *Paranthropus robustus* (Broom, 1938a) but the specific location from which it was recovered remains unknown, though ongoing fieldwork may help clarify its provenance (Thackeray et al., 2005; Braga et al., 2013; Braga et al., 2023; Braga and Thackeray, 2016).

Broom (1938a) first described the recovery of the left half of a subadult cranium (TM 1517a), an associated right mandibular corpus (TM 1517b), and several isolated teeth (TM 1517c) from a loose block that could not be securely linked to any specific breccia deposit and lay within roughly one yard of a small circular breccia exposure previously opened by lime workers. In subsequent work, Broom (1938b, 1942) attributed additional remains to the same individual– including the distal right humerus (TM 1517g), part of the proximal right ulna (TM 1517e), and several hand bones– which were reported as coming from “the same matrix as the skull and within a few feet of the spot where it was found” (Broom, 1938b: 897).

Continued excavations at Kromdraai, Sterkfontein, Swartkrans, Drimolen, Cooper’s, and Gondolin Caves have resulted in more discoveries of *P. robustus*, though TM 1517 remains to this day the only partial skeleton in which associated craniodental and postcranial elements are believed to represent a single individual (Thackeray et al., 2005; Braga and Thackeray, 2016; Cazenave et al., 2020). Originally, 12 postcranial fossils were associated with TM 1517, but Day and Thornton (1986) reassessed the assemblage and determined most of the elements were cercopithecoid. Currently, five TM 1517 fossils are identified as hominin: a talus (TM 1517d),

proximal ulna (TM 1517e), distal humerus (TM 1517g), and two distal phalanges (TM 1517k, o) (Skinner et al, 2013).

Subsequent work at Kromdraai led by Brain (1955-1956) yielded a hominin ilium (TM 1605) and excavations by Vrba (1977-1980) led to the discovery of a specimen (KB 5223) that was attributed by Braga & Thackeray, 2003 to *Homo*, but subsequent analyses have suggested that it represents *Paranthropus* (Lacruz, 2007; Grine et al., 2009; O'Hara and Guatelli-Steinberg, 2022; Zanolli et al., 2022), a view initially held by Grine (1982). Excavations at Kromdraai by Thackeray and colleagues (1993-2002) led to the discovery of a humeral shaft– the likely antimere of TM 1517g– and possible rediscovery of the type site of *P. robustus* (Thackeray et al., 2005). Additional postcranial fossils identified by that team (KB 542 [metacarpal], KB 3133 [cuboid], KB 3297 [calcaneus], KB 3601 [distal femur]) and hypothesized to be hominin (Thackeray et al., 2001) are either cercopithecoid or felid (Suzman, 1978; Skinner et al., 2013; Braga and Thackeray, 2016; DeSilva et al., 2018). These fossils discussed above are briefly described and pictured with information on how to access digital data in Skinner et al. (2013).

Renewed excavations began in 2014 by the Kromdraai Research Project (KRP) (Braga & Thackeray, 2016; Braga et al., 2017; Braga et al., 2022a) in a 900m^2 area north of Kromdraai B where previous scholars had focused their efforts. This northern "extension site" uncovered new breccia deposits and contributed to a revised stratigraphic understanding of the site (Bruxelles et al., 2016, Braga and Thackeray, 2016; Braga et al., 2017). It contains the oldest part of the Kromdraai stratigraphic sequence described so far — Units O and P — as illustrated in Braga et al. (2022a). Unit P is considered to be equivalent to the decalcified deposits that were designated as 'Member 2' and considered as "sterile" by Vrba (1981) (Braga et al., 2022a). Unit O is stratigraphically older that Unit P. Over six thousand faunal fossils have since been unearthed *in situ* (Fourvel et al., 2016; Fourvel et al., 2018; Pavia et al., 2020; Fourvel & Frerebeau, 2023;

Hanon et al., 2024; Pavia et al., 2025; Sambo et al., 2025). The KRP has found close to sixty hominin fossils, including 36 craniodental remains from *P. robustus* (Braga et al., 2017; Braga et al., 2021; Braga et al., 2022b; Braga et al., 2023; Braga & Grine 2024) and *Homo* aff. *erectus* (Braga & Moggi-Cecchi, 2025). The *Homo* KW 7000 juvenile mandible documented the presence of two hominin genera at Kromdraai (Braga & Moggi-Cecchi, 2025) as is the case at Swartkrans (reviewed in Grine, 2005) and Drimolen (Herries et al., 2020). The biochronological assessments of carnivore and bovid specimens recovered from Unit P consistently indicate an age predating 2 Ma for these assemblages (Fourvel et al. 2018; Hanon et al. 2024). If corroborated by additional geochronological evidence, the *P. robustus* and *Homo* aff. *erectus* specimens from Unit P at Kromdraai would present one of the earliest known occurrences of these taxa in southern Africa.

Here, we report 21 new postcranial fossils from Units O and P at Kromdraai (Table 1), not including a calcaneus (KW 6302) that has been previously described (Harper et al., 2022). At least 20 postcranial remains out of 21 described here securely derive from Unit P and are therefore considered contemporaneous within the currently recognized stratigraphic framework, although the precise chronology of Unit P remains under investigation. One fossil, a patella, may derive from the stratigraphically older Unit O.

While the fossils in Unit P are clustered in four distinct areas (Ngoloyi et al., 2020), there is no clear association between any craniodental and postcranial hominin remains thus far, making taxonomic attribution of isolated postcranial remains difficult. Table 1 presents a list of all hominin postcranial remains recovered to date from Kromdraai Unit P and possibly Unit O, including the new postcranial remains for which we provide anatomical descriptions, accompanied by functional interpretations and hypothesized taxonomic attribution where

possible. These taxonomic proposals are tentative and fall under the C-3 category (lowest level of confidence) established by Grine et al. (2022).

Methods and Results

Descriptions of postcranial fossils from Kromdraai, South Africa are organized below by anatomical region, starting with the upper limb and hand, proceeding to the lower limb and then the foot. Within each anatomical region, the fossils are organized by accession number. Each description begins with a characterization of the preservation, followed by the morphology of the bone. Comparative fossil material listed in the Tables is limited to Plio-Pleistocene fossils from South Africa >1Ma, and fossils from East Africa that bracket (~1.5-2.5 Ma) the roughly 2 Ma age of Kromdraai Unit P. Extant African ape and human samples vary by element and are detailed in the figure legends.

Upper Limb

Humeri

KW 6575 (Figure 2) is part of the shaft and distal end of a right humerus. The proximal end is sheared off, creating a jagged break and revealing the internal canal, which is infilled with sediment. Here, the exposed cortex is thickest medially. The distal end extends further on the medial side preserving the area just before the medial epicondyle. The corresponding area on the lateral side is missing and reveals exposed trabeculae. Posteriorly, a small superomedial portion of the olecranon fossa is preserved. A moderate longitudinal crack is found on the anteromedial surface of the shaft measuring about 35 mm in length. The entire bone measures 91.1 mm proximodistally (PD) and 33.3 mm mediolaterally (ML). There is a sharp, well-defined, lateral

supracondylar ridge. At the superior formation of the lateral supracondylar ridge, the humeral shaft measures 17.8 mm ML and 16.2 mm anteroposteriorly (AP). At the superior edge of the olecranon fossa, the humerus measures 27.2 mm ML and 11.5 mm AP.

KW 8246 (Figure 2; Table 2) is the distal end of a right humerus. The fossil is composed of two halves readhered in the midline. There is erosion along the lateral epicondyle and along the anterior aspect of the trochlea. The fossil measures 68.3 mm ML with a maximum of 29.3 mm AP. The capitulum is spherical and measures 19.7 mm PD and a maximum of 20.2 mm ML. The trochlea measures a maximum of 30.7 mm ML (measured inferiorly) and 26.2 mm PD (measured posteriorly). The AP thickness of the medial margin of the trochlea is 23.1 mm. The trochlea is inferiorly deeply grooved and exhibits a v-shape. The medial epicondyle is quite pronounced and extended medially measuring 15.3 mm AP and projecting 24.3 mm ML from the medial margin of the trochlea. The olecranon fossa is deep and measures 19.6 mm ML and 12.3 mm superoinferiorly (SI).

KW 9620 (Figure 2; Table 3) is the proximal end of a right humerus that includes the humeral head, greater tubercle, and part of the superior portion of the lesser tubercle. There is some sediment matrix adhered to the surface of the head, tubercle, and shaft. The fossil preserves slightly more of the shaft just inferior to the head and tubercle on the posterior surface extending approximately 13.9 mm from the posterolateral edge of the humeral head. Anteriorly, the fossil is missing much of the bone exposing trabeculae. The humeral head is elliptical in dorsal view and has a maximum SI height of 32.6 mm and maximum AP breadth of 32 mm. There is a marked groove between the humeral head and greater tubercle representing the anatomical neck. The greater tubercle is 26.2mm AP with a superiorly positioned rugosity for the insertion of *Mm.*

supraspinatus and *infraspinatus*. The preserved portion of the lesser tubercle measures 17.3 mm in ML width. There is a smooth area medially for the insertion of the *M. subscapularis*. About 5 mm of a relatively deep bicipital groove is preserved beginning from the anterolateral margin of the humeral head.

KW 9970 (Figure 2; Table 2) is the capitulum and trochlea of a right distal humerus. There is some brown sedimentary matrix adhered to parts of the surface. The anterior and posterior surfaces of the capitulum and trochlea are intact, but there is damage superiorly, medially, and laterally, exposing internal trabecular bone. The fossil measures 39.5 mm in total ML width and 19.4 mm in maximum PD height. The articular surface is 36.8 mm ML. The capitulum measures 17.7 mm PD and 14.0 mm ML at its widest aspect. A 3.4 mm ML zona conoidea separates the capitulum from the trochlea, which itself measures 20 mm ML and 17.8 mm PD. The depth of the trochlea is moderate and more U-shaped.

Manual phalanges

KW 6263 (Figure 2; Table 4) is an unsided manual intermediate phalanx. The bone is very well preserved, with no erosive surfaces. In lateral view, KW 6263 is relatively straight (and similar to the other intermediate phalanges from Kromdraai). In dorsal view, the shaft is ML broadest proximally and tapers distally. Palmarly, there are two well-developed and projecting semi-circular attachments for the flexor sheath that extend to the midshaft and there is no development of the median bar. These attachments are inset from the lateral edges of the shaft and closer to the ML midline than in KW 10582 or KW 12350 (or StW 331). The proximal end has two clear facets for the trochlea of the proximal phalanx and, unlike KW 10582, there is no projecting ‘beak’ at the dorsoproximal edge. The trochlea is slightly asymmetrical, suggesting, in

combination with its small size, it is possibly a left IP2 or right IP5. The bone is 19.4 mm in maximum PD length. The base is 9.0 mm ML and 6.9 mm DP and the trochlea 7.5 mm ML and 4.3 mm DP. At midshaft, the bone flattens and measures 6.3 mm ML and 3.6 mm DP.

KW 10582 (Figure 2; Table 4) is an unsided manual intermediate phalanx. There is erosion of the proximal articular surface, though enough is preserved to estimate its dimensions and two articular facets for the trochlea of the proximal phalanx are clear. The dorsoproximal edge of the shaft/facet extends proximally to form a 'beak'. Proximally and dorsally, there is a small osteophytic growth, perhaps resulting from a hyperextension injury. In lateral view, KW 10582 is relatively straight, even at the distal end, although the osteophytic growth obscures the assessment of the complete shaft. In dorsal view, the shaft is ML broadest at the proximal end and tapers distally. The trochlea is ML broader than the distal shaft and is not symmetrical. The median bar is poorly developed and only minimally projects palmarly at its more distal extent. The semi-circular insertions for the flexor sheaths project palmarly slightly, rather than being concave. The bone is 26.7 mm PD. The base is 11.5 mm ML and 8.5 mm DP and the trochlea is 8.5 mm ML and 4.8 mm DP. At midshaft, the bone flattens and measures 7.7 mm ML and 4.9 mm DP.

KW 12350 (Figure 2; Table 4) is an unsided manual intermediate phalanx. There is a small fragment missing from the palmar edge of the proximal facet but otherwise the bone is well-preserved. In dorsal view, the shaft is ML broadest at the proximal end and tapers distally. The trochlea is ML broader than the distal shaft and the articulation is slightly asymmetrical, suggesting, in combination with its short length, that it is from the second or fifth ray. Palmarly, there is one well-developed and projecting semi-circular attachment for the flexor sheath on the

right side while the other is only a slightly raised rugosity of the palmar surface, indicating asymmetrical muscular loading of this digit. There is no development of the median bar. The bone is 19.0 mm PD. The base is 10.6 mm ML and 7.5 mm DP. The head is 7.3 mm ML and 4.5 mm DP. At midshaft, the bone flattens and measures 6.3 mm ML and 4.0 mm DP.

KW 10379 (Figure 2; Table 5) is an unsided, non-pollical distal manual phalanx. There is some sediment attached to the bone on the proximopalmar surface and the dorsal surface of the distal edge of the apical tuft. There is a fragment missing from the palmar edge of the proximal articular facet. There are some moderate cracks on both the dorsal and plantar surfaces as well as the base, which may cause a small amount of distortion to the overall shape. The base is palmarly canted and the apical tuft is well-developed. The bone is 15.8 mm in maximum PD length. The base measures 10.7 mm ML and 6.2 mm DP and the apical tuft measures 7.5 mm ML and 4.7 mm DP. The shaft is ML narrower than the apical tuft and especially the base, measuring 5.3 mm ML and 4.5 mm DP.

KW 11130 (Figure 2; Table 5) is an unsided, non-pollical distal manual phalanx. The bone measures 14.3 mm in PD length. There is a small fragment missing from the midline of the palmar edge of the proximal facet and the cortical bone is eroded at the most distodorsal edge of the apical tuft. The proximal facet is oval measuring 9.8 mm ML and 6.1 mm DP. The apical tuft is well-developed both mediolaterally and dorsopalmarly, measuring 7.3 mm ML and 3.9 mm DP. The midshaft is ML narrower than both the proximal and distal ends, measuring 5.2 mm ML and 3.8 mm DP.

Lower Limb

Femora

KW 8120 (Figure 3; Table 6) is a left femur preserving two large pieces with PD heights of 102.2 mm and 140 mm respectively and one small shaft fragment without a clear fit to the others which measures 56.3 mm PD. The most proximal piece consists of approximately the upper third of the femur. The femoral head is missing and the greater and lesser trochanters are cleanly broken off with exposed trabeculae in all three areas. Some minor cracks are found longitudinally along the anterior and posterior surfaces. Distally, the piece is cleanly broken exposing the internal canal. The second large piece is a portion of the midshaft composed of three fragments glued together. It does not cleanly contact the proximal fragment. The piece is fragmented such that the full circumference of the bone is not complete in any location. Distally, the bone flares laterally suggesting it is approaching the lateral condyle; internally, trabecular bone is exposed. While this distally flared portion of fragment is intact, it is somewhat crushed and damaged and not a continuous smooth surface. The femoral neck is SI tall and AP compressed, measuring 27.1 mm SI and 18.3 mm AP. There is a subtle groove for the tendon of *m. obturator externus* along the posterior neck. A raised intertrochanteric crest is preserved for ~19.3 mm connecting the eroded trochanters. Anteriorly, the neck is smooth, with a subtle intertrochanteric line. The neck shaft angle is approximately 116° (range 114-118). There is slight femoral anteversion in the sagittal plane. The subtrochanteric shaft is platymeric, measuring 28.1 mm ML and 23.2 mm AP. Laterally, there is a raised gluteal tuberosity (third trochanter) which continues inferomedially as a gluteal line, lateral to which is a prominent hypotrochanteric fossa. Medially, the spiral line descends from the lesser trochanter inferodistally and approaches the gluteal line. The lines continue with some separation, however the necessary posterior fragment is missing to assess whether these lines ever merge into a linea

aspera. There is no observable nutrient foramen. At the break, the shaft measures 25.9 mm ML and 22.2 mm AP. The cortex is thick, measuring approximately 9.5 mm laterally, 8.7 mm medially, 7.6 mm anteriorly, and 7.8 mm posteriorly. There is no observable waisting of the shaft.

KW 9950 (Figure 3; Table 6) is a right femur. The fossil exists in three separate parts which preserve the proximal end and most of the shaft. They measure 56.3 mm SI, 95.7 mm SI, and 123.2 mm SI. The proximal most fragment preserves the femoral head and neck. The head has an area of erosion on the superior surface and some light erosion on the posteroinferior border of the head. There is a puncture just posterior to the fovea with a small crack proceeding from the puncture to the margin of the femoral head on the posterior surface. There are a few cracks along the posterior surface of the femoral neck near the border of the femoral head. The greater trochanter is missing, revealing some exposed trabeculae. The bone is sheared just superior to where the lesser trochanter would be. Two small, adjoining pieces have been glued back in place on the anterior surface just superior to where the bone is sheared. The second fragment contains the lesser trochanter and part of the shaft and conjoins with the first, though deformation of the articulating ends and displacement of some pieces prevents a clean connection. This piece is made of five fragments that have been pieced back together and therefore shows a number of cracks throughout. The lateral shaft extends distally while the anterior and medial portions are missing in this area. The third portion is a distal segment of the femoral shaft, approaching the missing condyles. This piece does not articulate with the distal portion of the second piece indicating that there is a missing portion of the shaft. The lateral aspect of the distal end is flared while the corresponding area on the medial aspect is missing. The entire broken distal end exposes trabecular bone. A few longitudinal cracks are also found along the shaft. Both the anterior and posterior surfaces of the fragment show some missing portions of the outermost

layer(s) of bone. The proximal portion of this segment is composed of four fragments that have been pieced back onto the shaft and therefore reveal a number of cracks. A number of smaller bone fragments are associated with KW 9950 but not attached. The femoral head is spherical with a prominent fovea. It measures 34.5 mm AP, 33.6 SI, 28.4 ML. The fovea measures 10.5 SI and 10.5 ML. The superior articular surface of the femoral head is perpendicular to the long axis of the neck. The femoral neck is SI tall and AP compressed, measuring 28.3 mm SI and 18.7 mm AP. The biomechanical neck length can be estimated from the lateral edge of the preserved shaft to the midpoint of the head and is approximately 68 mm. The morphological length of the neck from the intertrochanteric crest to the posterior articular surface of the head is 38.3 mm. There is a subtle groove for the tendon of *m. obturator externus* along the posterior neck. Anteriorly, the neck is smooth, with a barely detectable intertrochanteric line. The neck shaft angle is approximately 115° (range 112-118°). Because the proximal two fragments do not conjoin cleanly it is difficult to assess femoral anteversion, although it appears as though the head and neck are slightly torqued relative to the shaft. The lesser trochanter is set at an oblique angle with the inferior portion nearer the posterior surface and the superior portion angled toward the anterior surface. The lesser trochanter is longer SI (19.4 mm) than AP (10.8 mm) presenting an oval shape. There is a groove anterior and lateral to the lesser trochanter. The subtrochanteric shaft is only slightly platymeric, measuring 29.4 ML and 26 mm AP. Laterally, there is a hypotrochanteric fossa, medial to which runs a gluteal line. Medially, the spiral line descends from the lesser trochanter inferodistally and merges with a pectineal line ~25 mm from the inferior rim of the lesser trochanter. The conjoined lines continue distally and approach the gluteal line. There is no observable nutrient foramen. At the break, the lateral cortex is thick, measuring 9.9 mm (laterally). The distal shaft is round in shape, measuring approximately 24.8 mm ML and 23.8 mm AP. Distally, preserved along a small portion of the posterior shaft is a

prominent linea aspera. Distally, it splits and the lateral supracondylar line is palpable, but the medial is not detectable because of erosion. There is a depression on the posterior surface where the outermost layers of bone have flaked off.

Patella

KW 8182 (Figure 3; Table 7) is a well-preserved left patella. Some erosion is present on the proximal border of the base and inferior border near the apex. More significant erosion is found on the posterior aspect with the majority affecting the distal portion of the medial facet and the medial border of the bone. Exposed trabeculae is found in most areas where there is erosion. While the inferior edge exhibits some erosion, there is a portion intact suggesting that the margin of the inferior border would not have extended much farther distally. There are some foramina as well as vertical striations along the anterior aspect of the patella. The maximum ML width of the patella is 35.2 mm with a minimum PD height of 29.4 mm. The maximum AP thickness of the bone is 17.4 mm. Despite the erosion on the inferomedial and superior surfaces, the lateral facet appears to be larger in SI height and wider in ML width. There is a strong interfacet ridge that is both AP thick and ML wide. The lateral border is more rounded while the medial border has a sharper angle along the midpoint to the apex. While the apex is not as strongly pointed as is seen in modern humans, it is observable and more pointed than the rounded border typically seen in ape patellae. Both facets are slightly concave.

KW 11502 (Figure 3; Table 7) is a partially preserved right patella composed of several pieces refitted and glued back together. The anterior surface has some longitudinal striations running superoinferiorly. The proximal portion, or base, is missing and there is exposed trabeculae in this area. There is a large fragment missing that has created a moderate to large crack longitudinally through the entire bone travelling slightly medial to the midline. There is light erosion on the medial and lateral edges. On the anteromedial surface of the bone there is a small

divot that may be an area where a layer of bone has flaked away. The patella is quite thick anteroposteriorly showing a gradual increase in thickening toward the midline on the posterior surface. The lateral facet appears ML wider than the medial facet. The preserved proximodistal height of the bone is 22.8 mm– this is a minimum since a significant portion of the base is missing. The mediolateral width of the bone is approximately 25.4 mm and the anteroposterior thickness is 13.5 mm.

Tarsals

KW 6780 (Figure 4; Table 8) is a left intermediate cuneiform. The proximal, dorsal, and distal surfaces are the best preserved. Some minor cracks are found throughout the bone. There is some erosion along the lateral and medial surfaces particularly obscuring the facets for the medial cuneiform. A small area of erosion is also found proximally along the dorsolateral aspect of the bone. Plantarly, there is some erosion of the base exposing trabeculae. The bone is 12.6 mm PD, 11.4 mm ML, and a minimum of 13.2 mm DP. In lateral view, the proximal surface is angled plantodistally, as is the case in hominins. Proximally, the concave facet for the navicular is 10.8 mm ML and 13.2 mm DP. Distally, the facet for the second metatarsal is relatively flat, though there is some concavity ML and convexity DP– it measures approximately 12.2 mm DP and 10.2 mm ML.

KW 10699 (Figure 4; Table 9) is a complete, well-preserved right navicular. There is minimal erosion of the bone with a small area of exposed trabeculae on the medial edge of the lateral cuneiform facet. It is 30.3 mm ML and 17.6 mm DP. Proximally, the facet for the talar head is concave and measures 21.2 mm ML and 14.0 mm DP. The tuberosity is large, projecting 9.2 mm ML from the edge of the articular surface for the medial cuneiform and extending 17.6 mm PD

and 10.0 mm DP. The most lateral part of the navicular body is 8.9 mm PD. Plantarly, there is a rugosity for the plantar calcaneonavicular ligament. Distally, the facets for the cuneiforms are positioned in roughly the same coronal plane, though the lateral cuneiform facet is angled slightly plantarly relative to the others. The medial cuneiform facet is bulbous and convex, measuring 12.7 mm ML and 10.5 mm DP. The intermediate cuneiform facet is flat and measures 10.3 mm ML and 7.6 mm DP. The lateral cuneiform facet is concave and measures 11 mm ML and 9.4 mm DP.

KW 12330 (Figure 4; Table 10) is a right calcaneus. The bone preserves 39 mm PD from the cuboid facet to a break in the bone just proximal to the edge of the posterior talar facet. The tuber is not preserved at all. More cortical bone is preserved along the medial aspect of the bone than the lateral. The peroneal trochlea is not preserved– there is exposed trabecular bone in this region. There is extensive erosion around the rim of the cuboid facet. The anterior, middle, and posterior talar facets are preserved, with minimal erosion around the edges. The distal body extends 18.1 mm PD from the distal edge of the proximal talar facet and is approximately 20.2 mm DP tall distally. It drops to 17.4 mm tall at the base of the posterior talar facet. The posterior talar facet is convex. It is 21.6 mm PD long and estimated 16.0 mm ML wide. Medially, the anterior and middle talar facets are fused, concave, and 29.3 mm PD long and 12.8 mm ML at its widest point. Distally, the cuboid facet is flat plantarly, but becomes concave dorsomedially as the facet bends into a dorsal rim. Relative to the plantar base, the cuboid facet is slightly angled. Medially, the sustentaculum tali projects 15.6 mm ML from the body of the calcaneus. It is 19.4 mm PD and 9.6 mm DP thick. There is a wide, shallow groove under the sustentaculum for the tendon of *m. flexor hallucis longus*. Plantarly, there is a prominent tubercle for the short plantar

ligament. At the proximal break, the tuber (not preserved) would have been roughly 21.7 mm ML based on the preserved cortex.

Metatarsals

KW 6994 (Figure 4; Table 11) is a partial right third metatarsal preserving 38.5 mm PD of the proximal base and shaft. The base is eroded plantarly and laterally with some exposed trabeculae. There is an irregular break in the shaft which extends farther distally on the medial side than lateral. There are a few minor cracks found throughout the length of the shaft as well as a small hole on the dorsal surface approximately 22 mm from the proximal edge of the base. The base is flat and measures a maximum of 17.1 mm DP (as measured to the plantar tubercle) and 12.4 mm ML. The preserved facet for the lateral cuneiform is flat and measures 11.4 mm DP and 8.3 mm ML but these are minimums owing to the extensive erosion. Plantarly there is a large tubercle for the plantar ligaments. Medially, there is a dorsally positioned facet for the second metatarsal which is 6.9 mm DP and 5.3 mm PD. At the break in the shaft, the dimensions are 10.4 mm DP and 7.2 mm ML.

KW 10829 (Figure 4; Table 12) is a complete, well-preserved, right first metatarsal. There is erosion on the superior surface of the proximal end as well as the dorsomedial portion of the head with the latter area showing exposed trabeculae. The bone is 45.3 mm long. Proximally, the base is 18.5 mm SI and 13.3 mm DP. The base is concave mediolaterally and relatively flat dorsoplantarly. The articular facet for the medial cuneiform is a minimum of 15.7 mm DP and 10.3 mm ML. The lateral rim of the base extends proximally and there is a ~5 mm divot proximolaterally for the insertion of *m. peroneus longus*, dorsal to which is a small contact area for the second metatarsal. In lateral view, the dorsal surface of the shaft is straight while the plantar surface is concave from the base to the head. Midshaft dimensions are 9.0 mm ML and

18.9 mm DP. The head is domed above the surface of the shaft; the dorsal head is mediolaterally narrow. The maximum dimensions of the head are 14.3 mm DP and 13.4 mm ML. The head is neutrally positioned relative to the shaft with no discernable axial torsion. There are prominent grooves for the sesamoids of *m. flexor hallucis brevis* running between well-developed medial, lateral, and plantar cornua. The head measured without the cornua is 12.0 mm DP and 11.0 ML. Using the equation in Pontzer et al. (2010), the shaft robusticity is a human-like 6.1.

Pedal phalanges

KW 11666 (Figure 4; Table 13) is a likely right pedal proximal phalanx, determined by the distomedial to plantolateral angulation of the head. The shaft and the base are well preserved, but the lateral side of the head shows some erosion. In lateral view, KW 11666 is slightly curved. Plantarly, there are two well developed tubercles for the *m. interosseous* just distal to the base, which is dorsally canted 97°. The bone is a minimum of 19.4 mm, with damage to the head precluding a length measurement. The base measures 9.9 mm ML and 6.9 mm DP. At approximately midshaft, KW 11666 is 6.2 mm ML and 5.2 mm DP. The head is badly damaged– what is preserved measures 8.1 mm ML and 5.2 mm DP.

KW 12276 (Figure 4; Table 13) is a likely left fifth pedal proximal phalanx. The head is obliquely angled distomedially to proximolaterally, consistent with the left side. The bone is exceptionally short and the base also has a distomedial to proximolateral angulation, which can be found in human fifth proximal phalanges. It is well-preserved, with only moderate erosion along the medial rim of the head. KW 122276 is short and straight, measuring only 15.6mm in length. The base is dorsally canted 103° and measures 7.2 mm ML and 5.4 mm DP. At midshaft, the fossil tapers to 4.0 mm ML and 2.9 mm DP. The head expands to 5.6 mm ML and 3.6 mm DP and is slightly grooved, especially plantarly.

KW 11099 (Figure 4; Table 14) is a right hallucal distal phalanx. The distal head is eroded, showing exposed trabeculae, with a greater portion missing from the medial side. Part of the lateral plantar base is eroded as well. The bone is 16.8 mm PD. The base is 14.0 mm ML and 7.6 mm DP. In medial or lateral view, the plantar portion of the tuft deflects dorsally. The tuft is 10.0 mm ML and 4.4 mm DP. At midshaft, the bone is 8.5 mm ML and 5.3 mm DP. Plantarly, there is a large and deep insertion for *m. flexor hallucis longus* medial and lateral to which are tubercles for attachment of the collateral ligaments anchoring the proximal and distal phalanges. In dorsal view, there is weak lateral deflection of the bone relative to the base. In axial view, there is minimal head torsion relative to the base, approximately 5°.

Discussion

Below we provide functional and tentative taxonomic interpretations of the Kromdraai postcrania, organized by the upper limb, lower limb, and the foot. The discussion closes with some observations on body size, taphonomy, and recommendations for future work.

Upper Limb of the Kromdraai hominins

The fragmentary humeral head KW 9620 is not complete enough to make salient functional interpretations though it is noteworthy that the intertubercular (bicipital) groove appears deep, like the condition found in African apes, suggestive of strong biceps important for arm flexion during climbing. The head of KW 9620 is relatively small, comparable in size to the *A. sediba* MH2 female (Table 3). There is not enough diagnostic evidence preserved to make a taxonomic identification for this fossil.

Two distal humeri (KW 6575 and KW 8246), however, may be from *P. robustus* (Figure 5). Fossil *Homo* and *Paranthropus* tend to differ in their distal shaft cross-sectional geometries with *Homo erectus* and modern humans more rounded and *Paranthropus* more anteroposteriorly compressed (Susman et al., 2001; Lague, 2015). Notably, though, Susman et al. (2001) and Lague (2015) came to diametric conclusions regarding Swartkrans distal humeri SKX 10924, SK 26400, and SKX 19495 with the former study regarding SKX 10924 as *Homo* and the others *Paranthropus* and the latter study the exact opposite. Thus, caution is warranted in using this feature alone to draw taxonomic conclusions. Still, we note that KW 6575 is very similar to TM 1517 in diaphyseal cross-sectional geometry and distinct from early *Homo* (Figure 5), making an attribution to *P. robustus* a reasonable hypothesis. Additionally, the distal humerus KW 8246 shares with TM 1517g, a large biepicondylar width, wide coronoid fossa, a lateral epicondyle set high relative to the capitulum, and a strongly projecting medial epicondyle (Figure 5), indicative of strong digital flexors consistent with evidence from other regions of the skeleton for substantial climbing in the locomotor repertoire of *P. robustus* (Robinson, 1972; Proctor, 2010; Georgiou et al., 2020; Cazenave et al., 2026). Additionally, the ratio of the articular breadth to the biepicondylar width of KW 8246 (0.70) falls between *Pan* and *Gorilla*, and is high even for *Australopithecus* (data from Churchill et al., 2013).

A morphometric assessment of intermediate phalanx morphology reveals that within the Kromdraai sample, KW 10582 is absolutely PD longer, but relative to length, is the most gracile (Figure 6). In comparison, KW 12350 is the most robust, while its asymmetrical morphology suggests it is either from the second or fifth ray. Across our comparative sample, there is substantial overlap in the ML breadth (relative to total length) of the proximal base and trochlea and the Kromdraai phalanges span this range of morphological variation (Figure 6). In relative midshaft breadth, the Kromdraai intermediate phalanges are narrower than all Swartkrans

specimens and *P. boisei*, and are most similar to *A. sediba* and *A. africanus* (StW 331). However, the Kromdraai intermediate phalanges lack the distinct, projecting flexor sheath ridges found in *A. sediba* MH2 intermediate phalanges. Qualitatively, the Kromdraai intermediate phalanges are most similar in overall shape and their moderate degree of shaft curvature to StW 331 (*A. africanus*) and most Swartkrans specimens (*P. robustus/Homo*). The midshaft breadth to total length dimensions is more humanlike than either the Swartkrans specimens (Figure 6) or the newly reported intermediate phalanges DNH 63, 65, 66 from Drimolen (Orr et al., 2026) though together this sample spans the variation found in modern gorillas. Thus, the taxonomic attribution of the Kromdraai phalanges is unclear. Functionally, the morphology is consistent with other early hominin hands that show short fingers (relative to the length of the thumb) that would facilitate dexterity but appear more curved than that of humans, suggesting use of the hands for locomotor grasping as well.

Distal phalanges are rarely preserved in the fossil record and thus comparisons are limited. Both Kromdraai specimens are relatively ML broad both at the midshaft and the expansion of the apical tuft compared with distal phalanges from Swartkrans and fall within the range of variation found in *H. naledi* (Figure 7). Two distal non-pollical phalanges (D2679 and D3489) attributed to early *Homo* from Dmanisi, Georgia appear more gracile than the Kromdraai specimens but have yet to be formally described (Lordkipanidze et al. 2007). Functionally, the Kromdraai distal phalanges have ML expanded apical tufts that imply well-developed palmar pulp and other soft tissues that facilitate manipulation and pad-to-pad precision grips (Marzke, 1997).

Lower limb of the Kromdraai hominins

The SK 82 and SK 97 proximal femora from Swartkrans, South Africa have long been accepted as deriving from *P. robustus* (Napier, 1964; Robinson, 1972). Four additional proximal femora from Swartkrans (SK 3121, SKW 19, SWT1/HR-2b, SWT1/LB-2) have subsequently been discovered and regarded as probable *P. robustus* femora (Susman et al., 2001; Pickering et al., 2012; Pickering et al., 2025). However, it is important to recognize that none of these fossils were found in association with craniodental material and their *P. robustus* status remains speculative, assigned to the C-3 (lowest confidence level) category (Grine et al., 2022). However, operating under the assumption that these tentative taxonomic assignments turn out to be correct, there are patterns in the data that may help identify the Kromdraai femora. Compared with *Homo*, purported *Paranthropus* femora possess relatively small heads and long femoral necks that are anteroposteriorly compressed (Napier, 1964; Robinson, 1972; Ruff et al., 1995; Susman et al., 2001; Ruff et al., 2013). *P. boisei* possess these features and additionally can be identified by a strong bar of bone along the running from the base of the neck to the lesser trochanter called the “posteroinferior marginal ridge” (Ward et al., 2023). *Homo* femora tend to have larger heads, and shorter femoral necks that are rounder in cross-section (Ruff et al., 2013; Ward et al., 2015; Figure 8), though the small body size of *Homo habilis* partial skeletons OH 62 (Johanson et al., 1987) and KNM-ER 64061 (Grine et al., 2026) indicate that there is probably some overlap in these morphologies that will make distinguishing between *Paranthropus* and early *Homo* femora difficult until the discovery of lower limb remains in association with craniodental fossils in South Africa.

The Kromdraai femora (KW 8120 and KW 9950) align well with femora assumed to belong to *P. robustus* in having long, anteroposteriorly compressed femoral necks and, in KW 9950, a relatively small femoral head (Figures 8 and 9). Similar to the other femora assigned to *P. robustus*, the Kromdraai femora have a low neck-shaft angle, a weakly developed, but

palpable, obturator externus groove, a barely discernable intertrochanteric line, and a prominent third trochanter/hypotrochanteric fossa complex for the insertion of *m. gluteus maximus*.

Patellae

The Kromdraai patellae are human-like; neither specimen exhibits the relatively narrow, tall, and anteroposteriorly thick patellae characteristic of the enhanced forceful knee extension seen in quadrupedal monkeys, or the relatively AP thin patellae that characterize the more mobile knees of apes (Ward et al., 1995). Instead, both show elevated anteroposterior thickness relative to patellar height and breadth (Figure 10a), consistent with a knee extensor mechanism in which increased quadriceps moment arms facilitate torque production during weight-bearing extension (Pina et al., 2014). Functionally, these linear proportions suggest that both patellae were optimized for repeated knee extension under load, rather than extreme flexion-extension cycles or highly mobile knee postures.

Within this shared signal, KW 8182 is larger and plots closer to fossil *Homo* and modern humans, suggesting a more derived knee extensor configuration (Figure 10a). A relatively thick patella anteroposteriorly, without a corresponding increase in proximodistal height (Figure 10b), suggests enhanced quadriceps moment arm without the lever arm configuration associated with forceful extension from fully flexed knee positions (Pina et al., 2014). KW 11502 overlaps with a possible *P. robustus* patella (SKX 1084), *Australopithecus sediba*, and small bodied *Homo* (Figure 10a), making taxonomic attributions difficult.

The foot of the Kromdraai hominins

KW 6302 is a well-preserved fragment of a calcaneus preserving the tuber and the posterior talar facet that is described elsewhere (Harper et al., 2022). During the 2025 field

season, another calcaneal fragment (KW 12330) was recovered which preserves the distal portion from the posterior talar facet to the cuboid facet. The overlapping morphology of the two calcanei aligns reasonably well (Figure 11), though by no means do these represent the same individual. The more complete KW 6302 calcaneus is taxonomically ambiguous, though Harper et al. (2022) found that it was morphologically distinct enough from the Omo-33-74-896 calcaneus to conclude those fossils are from different taxa.

Like KW 6302, KW 12330 has a strongly convex posterior talar facet, recalling the morphology in *A. africanus* (StW 352) and *A. sediba* (U.W. 88-99), distinct from the flatter facet in *A. afarensis*. Additionally, the set to the calcaneocuboid joint in KW 6302 is moderately oblique, like that seen in other *Australopithecus* specimens and suggestive of a weakly developed lateral longitudinal arch (Berillon, 2003; Prang, 2015; Heard-Booth, 2017). However, interpreting this morphology is entirely dependent on how the angle between the cuboid facet and the calcaneus is measured. Following Berillon (2003), the cuboid facet and plantar aspect of the distal calcaneal body (which runs parallel to the long axis of the calcaneus) form a low, 93° angle, quite distinct from the 105° in the OH 8 calcaneus. However, Prang (2015) and Heard-Booth (2017) measured the cuboid facet relative to the entire plantar base of the calcaneus which includes a projecting medial plantar process. The most plantar aspect of the cuboid facet is not preserved in KW 12330, so we couldn't fit a plane to the joint following Prang (2015), but fitting a line to the preserved surface in lateral view yields a cuboid facet angle of 103.7°, within the range of both modern humans and gorillas (Prang, 2015). This value is nominally higher than the Omo calcaneus (99°) and remains lower than OH 8 (108°) though damage prevents us from knowing how projecting the medial plantar process would have been in that fossil. Furthermore, caution should be taken interpreting this latter measurement since it utilizes a composite of two different individuals.

The KW 10699 navicular possesses a morphology in many ways intermediate between African apes and humans (Figure 12). The angle between the talar and lateral cuneiform surfaces, a proxy for lateral navicular body pinching, positions KW 10699 between modern humans and modern apes, closest to the condition found in StW 573. Only OH 8, typically considered to be *Homo habilis*, is within the human interquartile range. Similarly, the convexity of the distal surfaces in KW 10699 indicates more midfoot mobility than modern humans or OH 8 (Figure 12). The relatively large, projecting tuberosity of KW 10699 suggests low medial arches, though plantar rugosities show that this hominin possessed a calcaneonavicular (spring) ligament which helped stiffen the foot during bipedal propulsion. While clear differences between KW 10699 and OH 8 might support the hypothesis that the former is from *Paranthropus* if the latter is from *Homo*, other naviculars from *Homo* (e.g. *H. naledi*, *H. floresiensis* [Jungers et al., 2009; Harcourt-Smith et al., 2015]) are surprisingly primitive in their morphology. The navicular, therefore, is a highly variable bone through evolutionary time and any taxonomic assignment is unwise without associated craniodental fossils.

The proximodistal elongation of the KW 6780 intermediate cuneiform aligns this bone with humans and other hominins compared with apes, consistent with some degree of midfoot rigidity during bipedalism (Figure 13). Similarly, the proximal surface for the navicular is weakly concave, a morphology shared with the OH 8 foot fossil. Ultimately, however, there is nothing taxonomically diagnostic about KW 6780.

KW 10829 is a small first metatarsal. The base is strongly concave and moderately sigmoidal in shape, unlike the flat base found in fossil and modern *Homo*. This morphology, like that found in first metatarsals SKX 5017 and SK 1813 (often attributed to *Paranthropus*), and the taxonomically uncertain DNH 115, suggests some mobility of the hallux (Proctor, 2010; Orr et al., 2026). But KW 10829 possesses a small contact facet on the lateral base for the Mt2 and

lacks the external torsion of the head indicating that the hallux may have been mobile but not divergent. In lateral view, the head of KW 10829 is dorsally domed, indicating propulsion during bipedal locomotion. However, like the condition in *Australopithecus* (A.L. 333-115, StW 562), possibly *Paranthropus* (SKX 5017, SK 1813), and early *Homo* (Dmanisi) the head appears to taper dorsally and is rounded. Thus, the base and the head morphology of KW 10829 recalls that of proposed *Paranthropus* fossils SKX 5017 and especially SK 1813. However, while these Swartkrans specimens are noteworthy for their exceptional shaft robusticity, KW 10829 is relatively gracile. It is possible, then, that shaft robusticity in *Paranthropus* was as variable as it is in modern humans (see Figure 14) and that KW 10829 and SKX 5017 are sampling the extremes of this variation. If so, then the use of this characteristic to align the similarly robust first metatarsal of OH 8 with *Paranthropus* instead of *Homo* (as proposed in DeSilva et al., 2019) is unfounded. Alternatively, the differences in shaft robusticity may be taxonomically informative, a testable proposition should a first metatarsal be discovered with associated *Paranthropus* or early *Homo* craniodental material.

A fragmentary third metatarsal (KW 6994) is hominin-like in possessing a tall base (Figure 15), hypothesized to stabilize and stiffen the midfoot during bipedal propulsion. All known hominins, including KW 6994, fall within the modern human distribution for this feature. There is nothing taxonomically diagnostic about KW 6994.

There are two proximal pedal phalanges (KW 11666 and KW 12276). KW 11666 is relatively robust, though damage to the head precludes a certain length measurement. KW 12276 is remarkably short. In fact, it is the shortest pedal phalanx known in the early hominin fossil record (Figure 16). As with the lateral pedal phalanx from Swartkrans SKX 16699 (Trinkaus and Patel, 2016), the small size, high dorsal canting angle, and straight-shafted morphology of KW 12276 appears to align this fossil with *Homo* but similar morphologies exist in a phalanx from *P.*

boisei (Mongle et al., 2025). We therefore hesitate to make a taxonomic assignment for KW 12276 until pedal phalanges associated with early *Homo* or *P. robustus* are unearthed.

The distal hallucal phalanx KW 11099 is similar in size and morphology to StW 617, a probable *A. africanus* hallucal distal phalanx from Sterkfontein, South Africa. Like in modern humans, the bone is short and stout, possesses a deep concavity for the tendon of *m. flexor hallucis longus* and is marked by a dorsal deflection of the plantar surface, reflective of toe-off during bipedal propulsion. KW 11099, like StW 617, is only slightly laterally angled and lacks the high axial torsion typical of modern humans and some fossil hominins (e.g. *H. naledi* [Harcourt-Smith et al., 2015]), suggesting a push-off mechanism that differed from *H. sapiens*. Like KW 11099, the OH 10 hallucal distal phalanx also possesses a weak lateral angle but has a more human-like axial torsion (13° measured by Day and Napier, 1966), consistent with its assignation to genus *Homo*. Given these observations, their age, and site of discovery, it is reasonable to suggest that the three distal hallucal phalanges StW 617, KW 11099, and OH 10 represent three genera *Australopithecus*, *Paranthropus*, and *Homo* respectively (Figure 17). Doing so, renders the status of TM 1517k, a purported hallucal distal phalanx from the type specimen of *P. robustus*, unclear. TM 1517k has been identified as a hominin hallucal distal phalanx by some (Day and Thornton, 1986; Skinner et al., 2013) and a pollical distal phalanx by others (Kivell et al., 2015; DeSilva et al., 2018) though Kivell et al. (2023) reassessed TM 1517k and concluded it was not a pollical distal phalanx. Day and Thornton (1986) observed that TM 1517k possesses moderate lateral angulation and strong, human-like axial torsion. But TM 1517k lacks the hour-glass shape of the hallucal distal phalanx in the other hominins, the base is markedly dorsoplantarly compressed, and the bone is strongly curved in the sagittal plane. It remains unclear if TM 1517k and KW 11099 represent normal variation along a temporal range of *P. robustus*, if these differences are of taxonomic and functional importance signaling

different uses of the hallux in these two hominins, or if TM 1517k may have been misidentified as a hominin hallucal distal phalanx.

Taphonomy and body size

During the last field seasons, a small number of juvenile hominin postcrania were recovered at Kromdraai. These are currently under study and are not included in this paper. This information is relevant given that all 21 hominin postcrania described here are adult whereas roughly half of the craniodental remains from Kromdraai Unit P are juvenile (Braga and Grine, 2024). Whether this is a result of predator activity (i.e. the postcrania of juveniles were fully consumed) remains unclear. Additionally, at this time in the Cradle, there is an approximately 19:1 ratio of *Paranthropus*:*Homo* (Braga et al., 2022a), consistent with the craniodental remains from Kromdraai (Braga and Grine, 2024; Braga and Moggi-Cecchi, 2025). Applying that ratio to the postcrania, we might expect approximately two fossils to be from *Homo*. Indeed, we find that the morphology of a patella (KW 8182) and a pedal phalanx (KW 12276) to be *Homo*-like but resist assigning these fossils to *Homo* since there is no confirmed patella from *P. robustus* and there exists overlapping pedal phalangeal morphology between *Homo* and *Paranthropus* (Figure 16). Comparisons between the Kromdraai postcrania and fossils from Swarktrans assumed to be *Paranthropus* make it reasonable to assign the distal humeri (KW 6575 and KW 8246) and femora (KW 8120 and KW 9950) to this taxon, though we do so with considerable caution. We must await the discovery of a more complete partial skeleton of *P. robustus* than TM 1517 to confidently assign any other isolated element.

Assuming our tentative taxonomic assignments are correct, the Kromdraai postcranial fossils present confounding ranges of body size for *P. robustus* (Table 15). There are now seven femoral heads argued to be from *Paranthropus*, with diameters ranging from 28.6 mm (SK 3121)

to 37.2 mm (SK 97). KW 9950 appears to cluster with SK 82 in the larger half of specimens, tentatively suggesting it belonged to a male. However, using the equations in Grabowski et al. (2015), KW 9950 was only 32.9 kg. Meanwhile, the dimensions of the KW 8246 distal humerus are consistent with an extremely large 66.4 kg individual. There are a number of distinct possibilities for interpreting this apparent discrepancy. First, these data may support extended male growth in *P. robustus*, as suggested by craniodental evidence (Lockwood et al., 2007). Dimorphism appears moderate among most individuals, but some exceptionally large males (e.g. KW 8246) were present. A second possibility is an unbalanced sex ratio within Unit P at Kromdraai with KW 8246 representing the only *P. robustus* male and the remaining fossils, including the 9950 femur, belonging to females. This scenario is consistent with the presence of notably small craniodental *P. robustus* specimens (e.g. KW 9000) within Unit P (Braga et al., 2022). However, how to interpret the distribution of femoral head diameters in fossils attributed to *Paranthropus* remains unclear (Figure 18). A third interpretation is that the equations in Grabowski et al. (2015) underestimate body size in fossil hominins. Using the equations in Ruff et al. 2020 and Ruff and Wood (2023), KW 9950 belonged to a larger, 43.6kg individual. More fossils, especially ones associated with craniodental remains and other postcranial elements, will help untangle these possible interpretations of size variation in *Paranthropus*.

Our team next plans to study the internal bony architecture of some of these elements, which should provide important functional and taxonomic information (e.g. Cazenave et al., 2017; Komza & Skinner, 2019; Georgiou et al., 2020, Cazenave et al., 2022). Meanwhile, excavations will continue at Kromdraai and future discoveries, combined with continued efforts at Drimolen, Swartkrans, Malapa, and Sterkfontein will seek to better understand the evolution and paleobiology of *Homo* and *Paranthropus* and the extinction of *Australopithecus* roughly 2.0 million years ago.

Acknowledgements

The authors are grateful to Adriaan Kruger Lotz, trustee of the Lotz Family Trust, and his family for their permission to undertake fieldwork at Kromdraai. We thank the South African Heritage Resource Agency and the Cradle of Humankind World Heritage Management Authority for their help with the ongoing Kromdraai hominin site excavation permit (ID: 3035, 3176 and 3888) issued to Jose Braga in collaboration with Bernhard Zipfel and Francis Thackeray. We thank the Evolutionary Studies Institute, University of the Witwatersrand, for curating fossils from Kromdraai. We thank Sifelani Jirah for access to specimens curated at the University of the Witwatersrand. We thank the curators at the Ditsong National Museum of Natural History, the Kenya National Museum, National Museum of Tanzania, and National Museum of Ethiopia for permission to study comparative material in their care over the years. We are grateful to C. Zollikofer and M. Ponce de Leon who provided a surface scan of the Dmanisi fossils and C. Prang for a scan of OH 10. We also thank all of the excavators and colleagues who have worked at the excavations at Kromdraai since 2014. This work has been supported by the French Ministry of Foreign Affairs, the Centre National de la Recherche Scientifique (CNRS), the Institut des Deserts et des Steppes (Paris), the 'Patrick Mathieu Recherche et Conseil' company, M. Bruno Maisonnier, M. Stephane Monceaux, the Institut Picot de Lapeyrouse (Toulouse) and the 'AESOP plus' programme of Erasmus Mundus (European Union).

References

Balter, V., Blichert-Toft, J., Braga, J., Telouk, P., Thackeray, F., & Albarède, F. (2008). U–Pb dating of fossil enamel from the Swartkrans Pleistocene hominid site, South Africa. *Earth and Planetary Science Letters*, *267*(1-2), 236-246.

Berillon, G. (2003). Assessing the longitudinal structure of the early hominid foot: a two-dimensional architecture analysis. *Human Evolution*, *18*(3), 113-122.

Braga, J., Thackeray, J. F., Dumoncel, J., Descouens, D., Bruxelles, L., Loubes, J. M., Kahn, J.L., Stampanoni, M., Bam, L., Hoffman, J., Spoor, F. (2013). A new partial temporal bone of a juvenile hominin from the site of Kromdraai B (South Africa). *Journal of Human Evolution*, *65*(4), 447-456.

Braga, J., Fourvel, J. B., Lans, B., Bruxelles, L., & Thackeray, J. F. (2016). Evolutionary, chrono-cultural and palaeoenvironmental backgrounds to the Kromdraai site: A regional perspective. In: Braga, J., Thackeray, F. (Eds.), *Kromdraai: A Birthplace of Paranthropus in the Cradle of Humankind*, 1-16.

Braga, J., Thackeray, J. F., Bruxelles, L., Dumoncel, J., & Fourvel, J. B. (2017). Stretching the time span of hominin evolution at Kromdraai (Gauteng, South Africa): Recent discoveries. *Comptes Rendus Palevol*, *16*(1), 58-70.

Braga, J., Thackeray, J. F., & Zipfel, B. (2022a). The Kromdraai early hominin-bearing site. A review of recent findings. *L'anthropologie*, *126*(4), 103054.

Braga, J., Chinamatira, G., Zipfel, B., & Zimmer, V. (2022b). New fossils from Kromdraai and Drimolen, South Africa, and their distinctiveness among *Paranthropus robustus*. *Scientific Reports*, *12*(1), 13956.

Braga, J., Wood, B. A., Zimmer, V. A., Moreno, B., Miller, C., Thackeray, J. F., Zipfel, B., & Grine, F. E. (2023). Hominin fossils from Kromdraai and Drimolen inform *Paranthropus robustus* craniofacial ontogeny. *Science Advances*, *9*(18), eade7165.

Braga, J., & Grine, F. E. (2024). New craniodental fossils of *Paranthropus robustus* from Kromdraai, South Africa (2014–2017 excavations). *Journal of Human Evolution*, *188*, 103481.

Braga, J., & Moggi-Cecchi, J. (2025). Infant craniofacial diversity in early pleistocene *Homo*. *Nature Communications*, *16*(1), 4796.

Braga, J., & Thackeray, J. F. (2003). Early *Homo* at Kromdraai B: probabilistic and morphological analysis of the lower dentition. *Comptes Rendus Palevol*, *2*(4), 269-279.

Braga, J., Thackeray, F. (Eds.). (2016). *Kromdraai: A birthplace of Paranthropus in the Cradle of Humankind*. African Sun Media.

Brain, C.K., (1958). The Transvaal ape-man-bearing cave deposits. *Trans. Mus. Mem.*, 13, 1-125.

Broom, R. (1938a). The pleistocene anthropoid apes of South Africa. *Nature*, *142*(3591), 377-379.

Broom, R. (1938b). Further evidence on the structure of the South African Pleistocene anthropoids. *Nature*, *142*(1938), 897-899.

Broom, R. (1942). The hand of the ape-man, Paranthropus robustus. *Nature*, *149*(3784), 513-514.

Broom, R. (1943). An ankle-bone of the ape-man, Paranthropus robustus. *Nature*, *152*(3867), 689-690.

Bruxelles, L., Maire, R., Couzens, R., Thackeray, J. F., & Braga, J. (2016). A revised stratigraphy of Kromdraai. In: Braga, J., Thackeray, F. (Eds.), *Kromdraai, a Birthplace of Paranthropus in the Cradle of Humankind*, 31-47.

Burgess, M. L., McFarlin, S. C., Mudakikwa, A., Cranfield, M. R., & Ruff, C. B. (2018). Body mass estimation in hominoids: Age and locomotor effects. *Journal of Human Evolution*, *115*, 36-46.

Cazenave, M., Braga, J., Oettlé, A., Thackeray, J. F., De Beer, F., Hoffman, J., Endalamaw, M., Redae, B.E., Puymerail, L., & Macchiarelli, R. (2017). Inner structural organization of the distal humerus in *Paranthropus* and *Homo*. *Comptes Rendus Palevol*, *16*(5-6), 521-532.

Cazenave, M., Oettlé, A., Thackeray, J. F., Nakatsukasa, M., De Beer, F., Hoffman, J., & Macchiarelli, R. (2019). The SKX 1084 hominin patella from Swartkrans Member 2, South Africa: An integrated analysis of its outer morphology and inner structure. *Comptes Rendus Palevol*, *18*(2), 223-235.

Cazenave, M., Dean, C., Zanolli, C., Oettlé, A. C., Hoffman, J., Tawane, M., Thackeray, F., & Macchiarelli, R. (2020). Reassessment of the TM 1517 odonto-postcranial assemblage from Kromdraai B, South Africa, and the maturational pattern of *Paranthropus robustus*. *American Journal of Physical Anthropology*, *172*(4), 714-722.

Cazenave, M., Pietrobelli, A., Luková, A., Bachmann, S., Caruana, M. V., Clarke, R. J., Dunmore, C.J., Hammond, A.S., Heaton, J.L., Heile, A.J., Hoffman, J., Kuman, K., Pahr, D.H., Smith, C.M., Stratford, D., Synek, A., Tsegai, Z.J., Kivell, T.L., Pickering, T.R., & Skinner, M. M. (2026). Swartkrans *Paranthropus* and Sterkfontein *Australopithecus* from southern Africa had different locomotor repertoires. *Proceedings of the National Academy of Sciences*, *123*(20), e2532193123.

Churchill, S. E., Holliday, T. W., Carlson, K. J., Jashashvili, T., Macias, M. E., Mathews, S., Sparling, T.L., Schmid, P., de Ruiter, D.J., & Berger, L. R. (2013). The upper limb of *Australopithecus sediba*. *Science*, *340*(6129), 1233477.

Churchill, S. E., Green, D. J., Feuerriegel, E. M., Macias, M. E., Matthews, S., Carlson, K. J., Schmid, P., & Berger, L. R. (2018). The shoulder, arm, and forearm of *Australopithecus sediba*. *PaleoAnthropology*, *2018*, 234-281.

Crompton, R. H., McClymont, J., Elton, S., Thorpe, S., Sellers, W., Heaton, J.,Pickering, T.R., Pataky, T., Carlson, K.J., Jashashvili, T. Beaudet, A., Bruxelles, L., Goh, E., Kuman, K., & Clarke, R. (2022). StW 573 *Australopithecus prometheus*: its significance for an australopith bauplan. *Folia Primatologica*, *92*(5-6), 243-275.

Day, M. H. (1986). *Guide to Fossil Man*. University of Chicago Press.

Day, M. H., & Napier, J. R. (1966). A hominid toe bone from bed 1, Olduvai Gorge, Tanzania. *Nature*, *211*(5052), 929-930.

Day, M. H., & Thornton, C. M. B. (1986). The extremity bones of *Paranthropus robustus* from Kromdraai B, East formation member 3, Republic of South Africa: a reappraisal. *Anthropos (Brno)*, *23*, 91-99.

de Graaff, G. (1961). On the fossil mammalian microfauna collected at Kromdraai by Draper in 1895. *South African Journal of Science*, *57*(9), 259-260.

De Groote, I., & Humphrey, L. T. (2011). Body mass and stature estimation based on the first metatarsal in humans. *American Journal of Physical Anthropology*, *144*(4), 625-632.

DeSilva, J. M., Holt, K. G., Churchill, S. E., Carlson, K. J., Walker, C. S., Zipfel, B., & Berger, L. R. (2013). The lower limb and mechanics of walking in *Australopithecus sediba*. *Science*, *340*(6129), 1232999.

DeSilva, J. M., Churchill, S. E., Zipfel, B., Walker, C. S., Sylvester, A. D., McNutt, E. J., Harcourt-Smith, W.E.H., Claxton, A.G., Carlson, K.J., & Berger, L. R. (2018). The Anatomy of the Lower Limb Skeleton of *Australopithecus sediba*. *PaleoAnthropology*, *2018*, 357-405.

DeSilva, J., McNutt, E., Benoit, J., & Zipfel, B. (2019). One small step: A review of Plio-Pleistocene hominin foot evolution. *American Journal of Physical Anthropology*, *168*, 63-140.

DeSilva, J., & Grabowski, M. (2020). Femur. In: Zipfel, B., Richmond, B., Ward, C.V. (Eds.), *Hominin Postcranial Remains from Sterkfontein, South Africa, 1936-1995*, Oxford University Press: pp 202.

Di Vincenzo, F., Rodriguez, L., Carretero, J. M., Collina, C., Geraads, D., Piperno, M., & Manzi, G. (2015). The massive fossil humerus from the Oldowan horizon of Gombore I, Melka Kunture (Ethiopia,> 1.39 Ma). *Quaternary Science Reviews*, *122*, 207-221.

Draper, D., 1896. Report of meeting, 8 April, 1895. Geological Society of South Africa. *Transactions of the Geological Survey of South Africa*, *1*, 11.

Fourvel, J. B., Brink, J., O'regan, H., Beaudet, A., & Pavia, M. (2016). Some preliminary interpretations of the oldest faunal assemblage from Kromdraai. In: Braga, J., Thackeray, F. (Eds.), *Kromdraai, a Birthplace of Paranthropus in the Cradle of Humankind*, pp 71-106.

Fourvel, J. B. (2018). *Civettictis braini* nov. sp. (Mammalia: Carnivora), a new viverrid from the hominin-bearing site of Kromdraai (Gauteng, South Africa). *Comptes Rendus Palevol*, *17*(6), 366-377.

Fourvel, J. B., & Frerebeau, N. (2023). A new canid species (Carnivora: Canidae) from the Plio-Pleistocene hominin-bearing site of Kromdraai (Cradle of Humankind, Gauteng, South Africa). *PalZ*, *97*(1), 163-177.

Georgiou, L., Dunmore, C. J., Bardo, A., Buck, L. T., Hublin, J. J., Pahr, D. H., Stratford, D., Synek, A., Kivell, T., & Skinner, M. M. (2020). Evidence for habitual climbing in a Pleistocene hominin in South Africa. *Proceedings of the National Academy of Sciences*, *117*(15), 8416-8423.

Gibbon, R. J., Pickering, T. R., Sutton, M. B., Heaton, J. L., Kuman, K., Clarke, R. J., Brain, C.K., & Granger, D. E. (2014). Cosmogenic nuclide burial dating of hominin-bearing Pleistocene cave deposits at Swartkrans, South Africa. *Quaternary Geochronology*, *24*, 10-15.

Grabowski, M., Hatala, K. G., Jungers, W. L., & Richmond, B. G. (2015). Body mass estimates of hominin fossils and the evolution of human body size. *Journal of Human Evolution*, *85*, 75-93.

Grabowski, M., Hatala, K. G., & Jungers, W. L. (2018). Body mass estimates of the earliest possible hominins and implications for the last common ancestor. *Journal of Human Evolution*, *122*, 84-92.

Green, D. J. (2020). Scapula, clavicle, and proximal humerus. In: Zipfel, B., Richmond, B., Ward, C.V. (Eds.), *Hominin Postcranial Remains from Sterkfontein, South Africa, 1936-1995*, Oxford University Press: pp 37.

Grine, F. E. (1982). A new juvenile hominid (Mammalia: Primates) from Member 3, Kromdraai Formation, Transvaal, South Africa. *Annals of the Transvaal Museum*, *33*(11), 165-239.

Grine, F. E. (2005). Early *Homo* at Swartkrans, South Africa: a review of the evidence and an evaluation of recently proposed morphs. *South African Journal of Science*, *101*(1), 43-52.

Grine, F. E., Smith, H. F., Heesy, C. P., & Smith, E. J. (2009). Phenetic affinities of Plio-Pleistocene *Homo* fossils from South Africa: molar cusp proportions. In *The First Humans–Origin and Early Evolution of the Genus Homo.* (pp. 49-62). Dordrecht: Springer Netherlands.

Grine, F. E., Mongle, C. S., Fleagle, J. G., & Hammond, A. S. (2022). The taxonomic attribution of African hominin postcrania from the Miocene through the Pleistocene: Associations and assumptions. *Journal of Human Evolution*, *173*, 103255.

Grine, F. E., Yang, D., Hammond, A. S., Jungers, W. L., Lague, M. R., Mongle, C. S., Pearson, O.M., Leakey, M.G., & Leakey, L. N. (2026). New partial skeleton of *Homo habilis* from the upper Burgi Member, Koobi Fora Formation, Ileret, Kenya. *The Anatomical Record*.

Hammond, A. S., Mavuso, S. S., Biernat, M., Braun, D. R., Jinnah, Z., Kuo, S., Melaku, S., Wemanya, S.N., Ndiema, E.K., Patterson, D.B., Uno, K.T., & Palcu, D. V. (2021). New hominin remains and revised context from the earliest *Homo erectus* locality in East Turkana, Kenya. *Nature Communications*, *12*(1), 1939.

Hanon, R., Fourvel, J. B., Sambo, R., Maringa, N., Steininger, C., Zipfel, B., & Braga, J. (2024). New fossil Bovidae (Mammalia: Artiodactyla) from Kromdraai Unit P, South Africa and their implication for biochronology and hominin palaeoecology. *Quaternary Science Reviews*, *331*, 108621.

Harcourt-Smith, W. E., Throckmorton, Z., Congdon, K. A., Zipfel, B., Deane, A. S., Drapeau, M. S., Churchill, S.E., Berger, L.R., & DeSilva, J. M. (2015). The foot of *Homo naledi*. *Nature Communications*, *6*(1), 1-8.

Harper, C. M., Zipfel, B., DeSilva, J. M., McNutt, E. J., Thackeray, F., & Braga, J. (2022). A new early hominin calcaneus from Kromdraai (South Africa). *Journal of Anatomy*, *241*(2), 500-517.

Heard-Booth, A. N. (2017). *Morphological and functional correlates of variation in the human longitudinal arch* (Doctoral dissertation).

Heaton, J. L., Pickering, T. R., Carlson, K. J., Crompton, R. H., Jashashvili, T., Beaudet, A., Bruxelles, L., Kuman, K., Heile, A.J., Stratford, D., & Clarke, R. J. (2019). The long limb bones of the StW 573 *Australopithecus* skeleton from Sterkfontein Member 2: Descriptions and proportions. *Journal of Human Evolution*, *133*, 167-197.

Herries, A. I., Martin, J. M., Leece, A. B., Adams, J. W., Boschian, G., Joannes-Boyau, R., Edwards, T.R., Mallett, T., Massey, J., Murszewski, A., Neubauer, S., Pickering, R., Strait, D.S., Armstrong, B.J., Baker, S., Caruana, M.V., Denham, T., Hellstrom, J., Moggi-Cecchi, J., Mokobane, S., Penzo-Kajewski, P., Rovinsky, D.S., Schwartz, G.T., Stammers, R.C., Wilson, C., Woodhead, J. & Menter, C. (2020). Contemporaneity of *Australopithecus*, *Paranthropus*, and early *Homo erectus* in South Africa. *Science*, *368*(6486), eaaw7293.

Johanson, D. C., Masao, F. T., Eck, G. G., White, T. D., Walter, R. C., Kimbel, W. H., ... & Suwa, G. (1987). New partial skeleton of *Homo habilis* from Olduvai Gorge, Tanzania. *Nature*, *327*(6119), 205-209.

Jungers, W. L., Harcourt-Smith, W. E., Wunderlich, R. E., Tocheri, M. W., Larson, S. G., Sutikna, T., Due, R.A., & Morwood, M. J. (2009). The foot of *Homo floresiensis*. *Nature*, *459*(7243), 81-84.

Kivell, T. L., Deane, A. S., Tocheri, M. W., Orr, C. M., Schmid, P., Hawks, J., Berger, L.R., & Churchill, S. E. (2015). The hand of *Homo naledi*. *Nature Communications*, *6*(1), 8431.

Kivell, T. L., Churchill, S. E., Kibii, J. M., Schmid, P., & Berger, L. R. (2018). The hand of *Australopithecus sediba*. *PaleoAnthropology*, 282-333.

Kivell, T. L., Ostrofsky, K. R., Richmond, B. G., & Drapeau, M. S. (2020). Metacarpals and manual phalanges. In: Zipfel, B., Richmond, B., Ward, C.V. (Eds.), *Hominin Postcranial Remains from Sterkfontein, South Africa, 1936-1995*, Oxford University Press: pp 106-143.

Kivell, T. L., Baraki, N., Lockwood, V., Williams-Hatala, E. M., & Wood, B. A. (2023). Form, function and evolution of the human hand. *American Journal of Biological Anthropology*, *181*, 6-57.

Komza, K., Skinner, M. M. (2019). First metatarsal trabecular bone structure in extant hominoids and Swartkrans hominins. *Journal of Human Evolution*, *131*, 1-21.

Lacruz, R. S. (2007). Enamel microstructure of the hominid KB 5223 from Kromdraai, South Africa. *American Journal of Physical Anthropology*, *132*(2), 175-182.

Lague, M. R. (2015). Taxonomic identification of Lower Pleistocene fossil hominins based on distal humeral diaphyseal cross-sectional shape. *PeerJ*, *3*, e1084.

Lague, M. R., & Jungers, W. L. (1996). Morphometric variation in Plio-Pleistocene hominid distal humeri. *American Journal of Physical Anthropology*, *101*(3), 401-427.

Lague, M. R., Richmond, B. G., Green, D. J., Braun, D. R., Harris, J. W., Mbua, E., & Chirchir, H. (2013). A new~ 1.5 Ma hominin distal humerus from Ileret, Kenya. *American Journal of Physical Anthropology*, *150*.

Lague, M. R., Chirchir, H., Green, D. J., Mbua, E., Harris, J. W., Braun, D. R., Griffin, N.L., & Richmond, B. G. (2019). Humeral anatomy of the KNM-ER 47000 upper limb skeleton from Ileret, Kenya: Implications for taxonomic identification. *Journal of Human Evolution*, *126*, 24-38.

Lague, M. R., & Menter, C. G. (2020). Distal humerus. In: Zipfel, B., Richmond, B., Ward, C.V. (Eds.), *Hominin Postcranial Remains from Sterkfontein, South Africa, 1936-1995*, Oxford University Press: pp 49.

Clark, W. L. G. (1947). Observations on the anatomy of the fossil Australopithecinae. *Journal of Anatomy*, *81*(Pt 3), 300.

Lockwood, C. A., Menter, C. G., Moggi-Cecchi, J., & Keyser, A. W. (2007). Extended male growth in a fossil hominin species. *Science*, *318*(5855), 1443-1446.

Lordkipanidze, D., Jashashvili, T., Vekua, A., De León, M. S. P., Zollikofer, C. P., Rightmire, G. P., Pontzer, H., Ferring, R., Oms, O., Tappen, M., Bukhsianidze, M., Agusti, J., Kahlke, R., Kiladze, G., Martinez-Navarro, B., Mouskhelishvili, Al, Nioradze, M., & Rook, L. (2007). Postcranial evidence from early *Homo* from Dmanisi, Georgia. *Nature*, *449*(7160), 305-310.

Malan, B. D. (1959). Early references to the Sterkfontein caves: Krugersdorp. *South African Journal of Science*, *55*(12), 321-324.

Marchi, D., Walker, C. S., Wei, P., Holliday, T. W., Churchill, S. E., Berger, L. R., & DeSilva, J. M. (2017). The thigh and leg of *Homo naledi*. *Journal of Human Evolution*, *104*, 174-204.

Marzke, M. W. (1997). Precision grips, hand morphology, and tools. *American Journal of Physical Anthropology*, *102*(1), 91-110.

McHenry, H. M. (1992). Body size and proportions in early hominids. *American Journal of Physical Anthropology*, *87*(4), 407-431.

McHenry, H. M., & Brown, C. C. (2008). Side steps: the erratic pattern of hominin postcranial change through time. *Journal of Human Evolution*, *55*(4), 639-651.

Mongle, C. S., Orr, C. M., Tocheri, M. W., Prang, T. C., Grine, F. E., Feibel, C., Patel, B.A., Laureijs, O., Hobbs, T.E., Maiolino, S., Rossie, J., Mbogo, W., Du Plessis, A., Lonyericho, J., Woto Huka, W., Sale, H., Umuro, A., Yirgudo, P., Dalacha, I., Kirinya, M., Linga, E., Loki, R., Longaye, A., Longaye, M., Lonyericho, E., Loyapan, I., Makudo, N., Nyete, C., Leakey, M.G., & Leakey, L. N. (2025). New fossils reveal the hand of *Paranthropus boisei*. *Nature*, 1-8.

Napier, J. R. (1964). The evolution of bipedal walking in the hominids. *Archives de Biologie*, *75*, 673-708.

Ngoloyi, N. M., Dumoncel, J., Thackeray, J. F., & Braga, J. (2020). A new method to evaluate 3D spatial patterns within early hominin-bearing sites. An example from Kromdraai (Gauteng Province, South Africa). *Journal of Archaeological Science: Reports*, *32*, 102376.

O'Hara, M. C., & Guatelli-Steinberg, D. (2022). Reconstructing tooth crown heights and enamel caps: A comparative test of three existing methods with recommendations for their use. *The Anatomical Record*, *305*(1), 123-143.

Orr, C. M., Baker, S. E., Hobbs, T. E., Lague, M. R., Leece, A. B., Martin, J. M., Nalley, T.K., Patel, B.A., Prang, T.C., Schwartz, G.T., Tocheri, M.W., Strait, D.S., & Herries, A. I. (2026). Hominin postcranial remains from Drimolen Main Quarry, South Africa. *The Anatomical Record*.

Partridge, T.C. (1982). Some preliminary observations on the stratigraphy and sedimentology of the Kromdraai B hominid site. *Palaeoecologica Africana. 15*, 3-12.

Pavia, M. (2020). Palaeoenvironmental reconstruction of the Cradle of Humankind during the Plio-Pleistocene transition, inferred from the analysis of fossil birds from Member 2 of the hominin-bearing site of Kromdraai (Gauteng, South Africa). *Quaternary Science Reviews*, *248*, 106532.

Pavia, M., Braga, J., Delfino, M., Kgasi, L., Manegold, A., Steininger, C., Zipfel, B., & Val, A. (2025). A new species of Lovebird (Aves, Psittaculidae, Agapornis) from the Plio-Pleistocene of the Cradle of Humankind (Gauteng, South Africa). *Geobios*, *90*, 133-142.

Pickering, T. R., Heaton, J. L., Clarke, R. J., Sutton, M. B., Brain, C. K., & Kuman, K. (2012). New hominid fossils from Member 1 of the Swartkrans formation, South Africa. *Journal of Human Evolution*, *62*(5), 618-628.

Pickering, R., Herries, A. I., Woodhead, J. D., Hellstrom, J. C., Green, H. E., Paul, B., Ritzman, T., Strait, D.S., Schoville, B.J., & Hancox, P. J. (2019). U–Pb-dated flowstones restrict South African early hominin record to dry climate phases. *Nature*, *565*(7738), 226-229.

Pickering, T. R., Heaton, J. L., Clarke, R. J., Stratford, D., & Heile, A. J. (2021). Hominin lower limb bones from Sterkfontein Caves, South Africa (1998-2003 excavations). *South African Journal of Science*, *117*(1-2), 1-10.

Pickering, T. R., Cazenave, M., Clarke, R. J., Heile, A. J., Caruana, M. V., Kuman, K., Stratford, D., Brain, C.K., & Heaton, J. L. (2025). First articulating os coxae, femur, and tibia of a small adult *Paranthropus robustus* from Member 1 (Hanging Remnant) of the Swartkrans Formation, South Africa. *Journal of Human Evolution*, *201*, 103647.

Pina, M., Almécija, S., Alba, D. M., O'Neill, M. C., & Moya-Sola, S. (2014). The Middle Miocene ape *Pierolapithecus catalaunicus* exhibits extant great ape-like morphometric affinities on its patella: Inferences on knee function and evolution. *PLoS One*, *9*(3), e91944.

Pontzer, H., Rolian, C., Rightmire, G. P., Jashashvili, T., de León, M. S. P., Lordkipanidze, D., & Zollikofer, C. P. (2010). Locomotor anatomy and biomechanics of the Dmanisi hominins. *Journal of Human Evolution*, *58*(6), 492-504.

Prang, T. C. (2015). Rearfoot posture of *Australopithecus sediba* and the evolution of the hominin longitudinal arch. *Scientific Reports*, *5*(1), 17677.

Proctor, D. J. (2010). Brief communication: Shape analysis of the MT 1 proximal articular surface in fossil hominins and shod and unshod *Homo*. *American Journal of Physical Anthropology*, *143*(4), 631-637.

Robinson, J. T. (1972). *Early Hominid Posture and Locomotion*. University of Chicago Press.

Ruff, C. B., & Higgins, R. (2013). Femoral neck structure and function in early hominins. *American Journal of Physical Anthropology*, *150*(4), 512-525.

Ruff, C. B., Squyres, N., & Junno, J. A. (2020). Body mass estimation in hominins from humeral articular dimensions. *American Journal of Physical Anthropology*, *173*(3), 480-499.

Ruff, C. B., & Wood, B. A. (2023). The estimation and evolution of hominin body mass. *Evolutionary Anthropology*, *32*(4), 223-237.

Sambo, R., Hanon, R., Maringa, N., Steininger, C., Zipfel, B., Braga, J., & Linchamps, P. (2025). Ecomorphological analysis of bovid remains from the Plio-Pleistocene hominin-bearing deposit of Unit P at Kromdraai, South Africa. *Journal of Archaeological Science*, *61*, 104871.

Skinner, M. M., Kivell, T. L., Potze, S., & Hublin, J. J. (2013). Microtomographic archive of fossil hominin specimens from Kromdraai B, South Africa. *Journal of Human Evolution*, *64*(5), 434-447.

Susman, R. L., & Brain, T. M. (1988). New first metatarsal (SKX 5017) from Swartkrans and the gait of *Paranthropus robustus*. *American Journal of Physical Anthropology*, *77*(1), 7-15.

Susman, R. L. (1989). New hominid fossils from the Swartkrans formation (1979–1986 excavations): postcranial specimens. *American Journal of Physical Anthropology*, *79*(4), 451-474.

Susman, R. L., de Ruiter, D., & Brain, C. K. (2001). Recently identified postcranial remains of *Paranthropus* and early *Homo* from Swartkrans Cave, South Africa. *Journal of Human Evolution*, *41*(6), 607-629.

Susman, R. L., & De Ruiter, D. J. (2004). New hominin first metatarsal (SK 1813) from Swartkrans. *Journal of Human Evolution*, *47*(3), 171-181.

Suzman, I. (1978). A fossil felid femur formerly considered to be hominid (Mammalia: Felidae). *Annals of the Transvaal Museum*, *31*(15), 185-187.

Thackeray, J. F., De Ruiter, D. J., Berger, L. R., & Van Der Merwe, N. J. (2001). Hominid fossils from Kromdraai: a revised list of specimens discovered since 1938. *Annals of the Transvaal Museum*, *38*(4), 43-56.

Thackeray, J. F., Braga, J., Sénégas, F., Gommery, D., Potze, S., & Senut, B. (2005). Discovery of a humerus shaft from Kromdraai B: part of the skeleton of the type specimen of *Paranthropus robustus* Broom, 1938?. *Annals of the Transvaal Museum*, *42*(1), 92-93.

Trinkaus, E., & Patel, B. A. (2016). An Early Pleistocene human pedal phalanx from Swartkrans, SKX 16699, and the antiquity of the human lateral forefoot. *Comptes Rendus Palevol*, *15*(8), 978-987.

Vrba, E. S. (1981). The Kromdraai australopithecine site revisited in 1980; recent investigations and results. *Annals of the Transvaal Museum*, *33*(3), 17-60.

Ward, C. V., Ruff, C. B., Walker, A., Teaford, M. F., Rose, M. D., & Nengo, I. O. (1995). Functional morphology of *Proconsul* patellas from Rusinga Island, Kenya, with implications for other Miocene-Pliocene catarrhines. *Journal of Human Evolution*, *29*(1), 1-19.

Ward, C. V., Feibel, C. S., Hammond, A. S., Leakey, L. N., Moffett, E. A., Plavcan, J. M., Skinner, M.M., Spoor, F., & Leakey, M. G. (2015). Associated ilium and femur from Koobi Fora, Kenya, and postcranial diversity in early *Homo*. *Journal of Human Evolution*, *81*, 48-67.

Ward, C. V., Hammond, A. S., Grine, F. E., Mongle, C. S., Lawrence, J., & Kimbel, W. H. (2023). Taxonomic attribution of the KNM-ER 1500 partial skeleton from the Burgi Member of the Koobi Fora Formation, Kenya. *Journal of Human Evolution*, *184*, 103426.

Zanolli, C., Davies, T. W., Joannes-Boyau, R., Beaudet, A., Bruxelles, L., de Beer, F., Hoffman, J., Hublin, J.-J., Jakata, K., Kgasi, L., Kullman, O., Macciarelli, R., Pan, L., Schrenk, F., Santos, F., Stratford, D., Tawane, M., Thackeray, F., Xing, S., Zipfel, B., & Skinner, M. M. (2022). Dental data challenge the ubiquitous presence of *Homo* in the Cradle of Humankind. *Proceedings of the National Academy of Sciences*, *119*(28), e2111212119.

Zipfel, B., & Wunderlich, R. (2020). Metatarsals and pedal phalanges. In: Zipfel, B., Richmond, B., Ward, C.V. (Eds.), *Hominin Postcranial Remains from Sterkfontein, South Africa, 1936-1995*, Oxford University Press: pp 289-305.

Figure legends

Figure 1. Location of the Cradle of Humankind, South Africa (top) and the position of Kromdraai relative to other hominin fossil-bearing localities (bottom). The map indicates three *Australopithecus*-bearing sites (blue) and five *Paranthropus*-bearing sites (dark-yellow). The site of Sterkfontein is depicted in blue because only a few isolated teeth attributed to *P. robustus* have been recorded from its Member 5 deposits.

Figure 2. Upper limb and hand elements described in this paper. A. Proximal humerus KW 9620 in anterior (left) and posterior (right) view; B. Distal humerus KW 6575 in anterior (left) and posterior (right) view; C. Distal humerus KW 8246 in anterior (left) and posterior (right) view; D. Distal humerus KW 9970 in anterior (left) and posterior (right) view; Manual intermediate phalanges KW 6263 (E); KW 10582 (F); KW 12350 (G); Manual distal phalanges KW 10379 (H); KW 11130 (I).Phalanges are all in dorsal (left) and palmar (right) views. Scale bar is 10mm.

Figure 3. Lower limb bones described in this paper. A: KW 8120 femur in posterior (left) and anterior (right) views; B: KW 9950 femur in posterior (left) and anterior (right) view. Fragments associated with KW 9950 are to the bottom right of the image; C: KW 8182 patella in anterior view; D: KW 11502 patella in anterior view. Scale bar is 10mm.

Figure 4. Foot bones described in this paper. A. KW 12330 calcaneus in dorsal (left), lateral (upper right), and distal (bottom right) views; B. KW 10699 navicular in dorsal (top) and proximal (bottom) views; C. KW 6780 intermediate cuneiform in dorsal (upper left), plantar (upper right) and medial (bottom) views. D. KW 10829 first metatarsal in proximal (left), dorsal (middle) and lateral (right) views. E. KW 6994 third metatarsal in dorsal (left) and medial (right) views. F. KW 11666 proximal pedal phalanx in dorsal (left) and plantar (right) views; G. KW

12276 proximal pedal phalanx in dorsal (left) and plantar (right) views; H. KW 11099 distal hallucal phalanx in dorsal (left) and plantar (right) views. Scale bar is 10mm.

Figure 5. Top: Kromdraai distal humerus KW 8246 (far right) compared with a modern human (left), early *Homo* (D4507; middle left) and *P. robustus* (TM 1517; middle right). Compared with modern humans and early *Homo*, KW 8246, like TM 1517, has a larger biepicondylar width (1), coronoid fossa (2), and lateral epicondyle (3). Bottom: In cross-section, KW 6575 is *P. robustus*-like in having an anteroposteriorly flatter distal shaft (4) though it has a more human-like supracondylar crest (5).

Figure 6. Manual intermediate phalanx morphology from rays 2-5. Box-and-whisker plots of proximal base, midshaft and trochlear mediolateral breadth relative to total proximodistal bone length. 'SKX' includes n=6 specimens from Swartkrans (SKX 5019, 5021, 9449, 13476, 35439 and 36712) attributed to either *P. robustus* or early *Homo*; *H. naledi* (n=10) includes all complete intermediate phalanges within the sample (data from Kivell et al., 2015), including those of Hand 1; *A. sediba* (n=4) from MH2; KNM-ER 101000-035 is the only complete IP within this *P. boisei* hand, attributed to the third ray (Mongle et al., 2025). Extant samples from *Gorilla* (N=9), *Pan* (N=8), and *Homo sapiens* (N=21).

Figure 7. Manual non-pollical distal phalanges from rays 2-5. Box-and-whisker plots of midshaft and apical tuft ML breadth relative to total DP length. 'SKX' includes two specimens from Swartkrans (SKX 8963 and 27504); *H. naledi* (n=6) includes all complete distal phalanges, including those from Hand 1; TM1517o has also been suggested to be a cercopithecoid pedal hallucal phalanx (Day and Thornton, 1986). Data from Kivell et al., 2015.

Figure 8. Kromdraai femora (KW 8120 and KW 9950) share with *Paranthropus* and *Australopithecus* a long, anteroposteriorly (AP) compressed femoral neck and a small femoral head. Eastern African *Paranthropus* femora tend to have a prominent ridge along the inferior neck of the femur advancing to the lesser trochanter, indicated here on KNM-ER 3728 (see also Ward et al., 2023). This feature is underdeveloped on the Kromdraai and Swartkrans femora assigned to *P. robustus*. Fossil and modern *Homo* femora are characterized by a shorter, rounder neck and a relatively larger femoral head. Femora illustrated here in posterior view have been scaled such that the shaft dimensions are roughly the same size. KW 8120 and KNM-ER 3728 have been mirrored so that all femora are from the right side.

Figure 9. Neck shape index (AP/SI*100) in fossil hominins and modern humans (N=58). In general, early hominins, including *Paranthropus* have anteroposteriorly compressed femoral necks whereas fossil and modern *Homo* have rounder necks in cross-section. Both KW 8120 and KW 9950 possess AP compressed necks, supporting their attribution to *P. robustus*.

Figure 10. (a) Both KW 8182 and KW 11502 exhibit anteroposteriorly thick patellae relative to mediolateral width, a pattern shared with many early *Homo* specimens and *Papio* and consistent

with a knee mechanism favoring extension from a flexed position. (b) KW 8182 displays a disproportionately thick anteroposterior dimension relative to proximodistal height compared to all other taxa. In this metric it most closely resembles early *Homo*. Image of KW 8182 from superior view in top left of graph. Extant samples from *Papio* (N=9), *Pongo* (N=13), *Gorilla* (N=23), *Pan* (N=21), and *Homo sapiens* (N=9).

Figure 11. Calcaneus composite in lateral (A), medial (B), and superior (C) views, created by aligning KW 6302 (gray) and KW 12330 (turquoise). KW 12330 is shown at original scale; KW 6302 has been scaled up by a factor of 1.14.

Figure 12. Angles between the talar and lateral cuneiform articular surfaces (A), and between the lateral and medial cuneiform articular surfaces (B) across African apes, humans, and fossil hominins. (A) reflects the degree of anteroposterior pinching on the lateral side of the navicular. African apes exhibit the most pinched lateral border and humans the least. KW 10699 is intermediate between humans and African apes. (B) quantifies the convexity of the distal articular surfaces in relation to one another. African apes show a more convex distal surface, and humans a flatter one. KW 10699 falls at the lower end of the ape range and above the human range, indicating a more convex distal navicular surface than in humans. For both angles, KW 10699 most closely resembles StW 573. Extant samples from *Gorilla* (N=27), *Pan* (N=20), *Homo sapiens* (N=20).

Figure 13. The intermediate cuneiform in humans is proximodistally elongated compared with its ML width. This morphology is hypothesized to contribute to the stiffness of the midfoot during heel lift. KW 6780 falls within the human range along with OH 8 and, to a lesser degree, StW 573. Extant samples from *Gorilla* (N=39), *Pan* (N=74), and *Homo sapiens* (N=43).

Figure 14. Modern human first metatarsal shaft robusticity is quite variable, but is higher than African apes, on average. Because of their short length and dorsoplantarly tall midshafts, purported *P. robustus* first metatarsals SK 1813 and SKX 5017 are exceptionally robust, beyond the range found in modern humans. In contrast, the KW 10829 first metatarsal is more gracile. It is noteworthy that the range of values in robusticity among hominins from Swartkrans, Sterkfontein, Olduvai, Dmanisi, and Kromdraai can be incorporated within the range of humans today. Extant samples from *Gorilla* (N=22), *Pan* (N=60), and *Homo sapiens* (N=110). Right: SK 1813, SKX 5017 (mirrored) and KW 10829. Scale bar is 1cm.

Figure 15. The base of the third metatarsal is dorsoplantarly tall in hominins compared with African great apes. For this measure, KW 6994 is within the human and fossil hominin range. Extant samples from *Gorilla* (N=13), *Pan* (N=12), and *Homo sapiens* (N=25).

Figure 16. Length and dorsal canting in hominin proximal pedal phalanges (rays 2-5). *Australopithecus* (in red) tend to have longer proximal pedal phalanges with less dorsal canting whereas fossil *Homo* and *Paranthropus* (KNM-ER 101000) have shorter phalanges with more

dorsal canting. KW 12276 has *Homo*-like dorsal canting and is strikingly small, probably because it is from a fifth digit which is a poorly sampled in the fossil record. Data from Trinkaus and Patel, 2016; DeSilva et al., 2019; Mongle et al., 2025; Orr et al., 2026.

Figure 17. Top: KW 11099 in, from left to right, dorsal, plantar, and distal views; bottom: TM 1517k. Although TM 1517k possesses axial torsion, it differs from KW 11099 in having a dorsoplantarly narrower base, sagittal plane curvature, and more of a tuft like morphology to the distal end. StW 617 (*A. africanus*) and OH 10 (*H. habilis*) are shown in the top and bottom right respectively for comparison.

Figure 18. Femoral head diameter in South African hominins from Kromdraai, Sterkfontein, Swartkrans, Makapansgat, and Malapa. *Australopithecus* femora in white; *Paranthropus* in gray. Possible *Paranthropus* specimen (StW 311) in checkered gray. KW 8120 femur in black. Note that its size aligns well with other purported *Paranthropus* fossils SK 82 and StW1/LB-2, considerably larger than possible *Paranthropus* individuals SWT1/HB-2b, SKW 19, and SK 3121. This could indicate size dimorphism in *Paranthropus* tentatively supporting the assignation of KW 8120 as a male *P. robustus*. Data from DeSilva et al., 2012; Pickering et al., 2012; Ward et al., 2015; Heaton et al., 2019; DeSilva & Grabowski, 2020; Pickering et al., 2021; Ward et al., 2023; Pickering et al., 2025 and measurements taken on original specimens.

Tables

Table 1. Hominin postcranial remains from Kromdraai, South Africa

Catalogue #	Element	Side	+Geological unit	Species (if known)	Reference
TM 1517d	Talus	right	*Ex-situ* (possibly Unit X), 1938	*Paranthropus robustus*	Broom, 1943
TM 1517e	Proximal ulna	right	*Ex-situ* (possibly Unit X), 1938	*P. robustus*	Broom, 1938; Broom, 1942, Le Gros Clark, 1947
TM 1517g	Distal humerus	right	*Ex-situ* (possibly Unit X), 1938	*P. robustus*	Broom, 1938; Broom, 1942, Le Gros Clark, 1947
TM 1517k	Hallucal distal phalanx	left	*Ex-situ* (possibly Unit X), 1942	*P. robustus*	Day, 1986; Day and Thornton, 1986
TM 1517o	Distal manual	unsided	Ex-situ, 1942	Possible *P.*	Broom, 1942;

	phalanx			*robustus*	Day, 1986; Skinner et al., 2013 (but see Day and Thorton, 1986)
TM 1605	Ilium	left	Decalcified breccia, Unprovenienced (1955-56)	Hominin	Robinson, 1972
KB 5522	Humeral shaft fragment	left - likely antimere to TM 1517g	Possibly Unit X, 2002	*P. robustus*	Thackeray et al., 2005
KW 6263	Manual intermediate phalanx	unsided	Unit P	Hominin	This study
KW 6302	Calcaneus	left	Unit P	Hominin	Harper et al., 2022
KW 6575	Distal humeral shaft	right	Unit P	*P. robustus*?	This study
KW 6780	Intermediate cuneiform	left	Unit P	Hominin	This study
KW 6994	Proximal third metatarsal	right	Unit P	Hominin	This study
KW 8120	Femur	left	Unit P	*P. robustus*?	This study
KW 8182	Patella	left	Unit P	Hominin	This study
KW 8246	Distal humerus	right	Unit P	*P. robustus*?	This study
KW 9620	Proximal humerus	right	Unit P	Hominin	This study
KW 9950	Femur	right	Unit P	*P. robustus*?	This study
KW 9970	Distal humerus	right	Unit P	Hominin	This study
KW 10379	Manual distal phalanx	unsided	Unit P	Hominin	This study
KW 10582	Manual intermediate phalanx	unsided	Unit P	Hominin	This study
KW 10699	Navicular	right	Unit P	Hominin	This study
KW 10829	First metatarsal	right	Unit P	Hominin	This study
KW 11099	Hallucal distal phalanx	right	Unit P	Hominin	This study
KW 11130	Distal manual phalanx	unsided	Unit P	Hominin	This study

KW 11502	Patella	right	Unit P? Unit O?	Hominin	This study
KW 11666	Proximal pedal phalanx	right	Unit P	Hominin	This study
KW 12276	Proximal pedal phalanx	left	Unit P	Hominin	This study
KW 12330	Calcaneus	right	Unit P	Hominin	This study
KW 12350	Intermediate manual phalanx	unsided	Unit P	Hominin	This study

1+Unit P is the geological equivalent of Member 2 (Partridge, 1982; Bruxelles et al., 2016), and
2Pink Breccia (Brain, 1958). See Braga et al., 2022a for more details on the geological context of
3these fossils.
4
5
6Table 2. Distal humeral measurements (in mm)

	Taxon	Age	Biepicondylar breadth (ML)	Articular width (ML)	Capitulum width (ML)	Capitulum height (SI)	Minimum trochlear thickness (AP)	Lateral pillar	Medial pillar	Olecranon fossa width (ML)	Size (Geomean)
KW 8246	*P. robustus?*	≥2.0	68.3	48.0	20.2	19.7	12.5	17.3 (min)	13.0	19.6	22.8
KW 9970	Hominin	≥2.0	-	36.8	14.0	-	14.3	-	-	-	-
StW 573	*A. prometheus*	3.67	54.0	40.0	14.9	17.6	13.8	14.7	9.0	20.0 (est)	19.5
StW 431	*A. africanus*	2.0-2.6	59.2	40.6	13.4	17.6	15.7	16.1	-	19.6	-
KNM-ER 64061	*H. habilis*	2.0	-	-	14.1	18.0	-	-	12.6	-	-
DNH 32	*P. robus*	~2.0	43.3	32.8	12.5	16.5	12.2	14.4	8.2	17.9	17.2

	tus										
MH2	*A. sediba*	1.98	50.0	32.4	12.3	15.1	13.2	14.1	7.7	19.6	17.4
SKX 24600	*Homo?*	*1.8-2.25	44.6	32.4	12.4	16.3	11.3	10.7	9.3	20.2	16.9
KNM-ER 1504	*P. boisei*	1.9	59.9	39.5	14.0	17.9	10.4 (est)	17.5	14.0	21.5	20.6
KNM-ER 3735	*H. habilis*	1.9	57.4 (est)	32.3	11.8 (est)	16.4 (est)	12.0	15.0	10.2	25.4	19.0
KNM-ER 6020	*P. boisei*	1.8	75.3 (est)	44.7	17.0	23.8	16.7 (est)	20.8 (est)	14.3 (est)	27.5 (est)	25.6
TM 1517	*P. robustus*	1.4-1.8	51.5	39.2	15.7	16.2	12.9	14.0	9.7	18.3	18.9
KNM-ER 739	*P. boisei*	1.5	70.6	47.3	18.3	24.3	13.6	20.0	13.8	28.4	25.1
SKX 10924	*P. robustus?*	*~1.0	43.4	32.5	12.5	13.7	10.7	10.7	7.8	18.8	15.9

Data from Robinson, 1972; Lague and Jungers, 1996; McHenry and Brown, 2008; DiVincenzo et al., 2015; Churchill et al., 2018; Heaton et al., 2019; Lague & Mentor, 2020; Ruff et al., 2020; Grine et al., 2026; Orr et al., 2026 and measurements taken on original specimens.

*Here and elsewhere, Swartkrans dates are listed as: Member 1 Lower Bank (1.8-2.25 Ma); Member 1 Hanging Remnant (1.8-1.9 Ma); Member 2 (~1.4 Ma); Member 3 (~1.0 Ma) following Balter et al., 2008; Gibbon et al., 2014; Pickering et al., 2019.

Table 3. Proximal humeral measurements (in mm)

Catalogue #	**Taxon**	**Age (Ma)**	**Max. SI of head**	**Max. AP of head**	**Humeral head size (SI*AP)^0.5**
KW 9620	Hominin	≥2.0	32.6	32.0	32.3

Sts 7a	*A. africanus*	2.0-2.6	40.3	39.2	39.8
StW 328	*A. africanus*	2.0-2.6	33.4	28.5	30.9
StW 517	*A. africanus*	2.0-2.6	36.2	34.6	35.4
Omo 119-73-2718	Hominin	2.4	40	36.0	38.0
KNM-ER 1473	Hominin	2.04	44	43.7	43.9
MH2	*A. sediba*	1.98	33.0	31.8	32.4

1 Data from Ruff et al., 2020; Green, 2020 and measurements taken on original specimens.
2
3 Table 4. Manual intermediate phalanx measurements (in mm)

Catalogue #	Taxon	Age	Maximum length	Base ML	Base DP	Midshaft ML	Midshaft DP	Trochlea ML	Trochlea DP
KW 6263	Hominin	≥2.0	19.4	9.0	6.9	6.3	3.6	7.5	4.3
KW 10582	Hominin	≥2.0	26.7	11.5	8.5	7.7	4.9	8.5	4.8
KW 12350	Hominin	≥2.0	19.0	10.6	7.5	6.3	4.0	7.3	4.5
StW 331	*A. africanus*	2.0-2.6	30.3	13.1	9.9	9.3	5.6	8.8	6.2
StW 620	*A. africanus*	2.0-2.6	19.5	9.5	7.8	6.8	5.1	6.7	4.2
StW 635	*A. africanus*	2.0-2.6	25.4	10.6	8.8	8.2	4.8	7.7	4.7
StW 657	*A. africanus*	2.0-2.6	28.5	12.1	9.5	9.4	5.6	7.8	5.2
DNH 63	Hominin	~2.0	21.7	9.9	7.8	7.3	5.3	7.9	4.9

DNH 65	Hominin	~2.0	18.2	9.9	7.5	7.4	4.9	8.0	4.3
DNH 66	Hominin	~2.0	22.9	10.5	7.4	7.3	4.6	7.2	4.4
U.W. 88-122	*A. sediba*	1.98	21.6	10	-	6.9	4.1	7.8	4.8 (est)
U.W. 88-123	*A. sediba*	1.98	18.3 (est)	9.8 (est)	-	6.7 (est)	-	7.1 (est)	-
U.W. 88-161	*A. sediba*	1.98	22.2	9.7	8.7	6.3	5	8	4.9
U.W. 88-162	*A. sediba*	1.98	17.5	8.9	-	5.2	3.9	6.9	3.8 (est)
SKX 5019	Hominin	1.8-2.25	17.5 (est)	9.8	7.7	7.2	4.5	7.9 (est)	5.0 (est)
SKX 5021	Hominin	1.8-2.25	26.4	12.1	9.3	9.2	6.1	9.5	6.5
SKX 9449	Hominin	1.8-2.25	19.2	10.5	7.5	8.2	4.6	7.3	4.6
SKX 13476	Hominin	1.8-2.25	19.6	10.9	7.4	6.8	4.0	7.8	4.4
KNM-ER 101000-034	*P. boisei*	1.52	-	14.1	9.4	11.9	5.3	-	-
KNM-ER 101000-035	*P. boisei*	1.52	27.9	13.5	8.1	12.0	5.0	9.0	5.3
KNM-ER 101000-036	*P. boisei*	1.52	-	13.1	9.4	11.9	5.2	-	-
KNM-ER 101000-038	*P. boisei*	1.52	-	12.7	8.3	10.1	4.4	-	-

SKX 35439	Hominin	~1.0	20.7	10.9	7.7	7.6	4.7	7.2	4.5
SKX 36712	Hominin	~1.0	21.8	12.6	8.8	8.6	5.7	8.2	5.4

Data from Susman, 1989; Kivell et al., 2018; Kivell et al., 2020; Mongle et al., 2025; Orr et al., 2026 and measurements taken on original specimens.

Table 5. Manual distal phalanx measurements (in mm)

Catalogue #	Taxon	Age	Maximum length	Base ML	Base DP	Midshaft ML	Midshaft DP	Apical tuft ML	Apical tuft DP
KW 10379	Hominin	≥2.0	15.8	10.7	6.2	5.3	4.5	7.5	4.7
KW 11130	Hominin	≥2.0	14.3	9.8	6.1	5.2	3.8	7.3	3.9
StW 661	*A. africanus*	2.0-2.6	14.0	8.8	5.6	3.8	3.7	5.7	3.6
SKX 8963	Hominin	1.8-2.25	-	-	-	-	4.0	6.3	3.3
U.W. 88-124	*A. sediba*	1.98	16.0 (est)	-	-	5.1	5	7.7 (est)	4.4
TM1517o	*P. robustus*	1.4-1.8	12.7	8.4	5.2	5.3	3.4	5.7	2.9
SKX 27504	*Paranthropus*?	~1.0	14.0	6.8 (est)	6.0	3.8	-	5.5 (est)	-

Data from Susman et al., 1988; Kivell et al., 2018; Kivell et al., 2020 and measurements taken on original specimens.

Table 6. Proximal femora measurements (in mm)

Catalogue #	Taxon	Age (Ma)	Head diameter (max)	Neck height (SI)	Neck width (AP)	Subtrochanteric width	Subtrochanteric breadth	Neck shaft angle

						(ML)	(AP)	
KW 8120	*P. robustus* ?	≥2.0	-	27.1	18.3	28.1	23.2	116
KW 9950	*P. robustus* ?	≥2.0	34.5	28.3	18.7	29.4	26.0	115
StW 573n (right femur)	*A. prometheus*	3.67	35.2 (est)	25.2	18.3	27.8	21.6	125
StW 598	*A. africanus*	3.67?	32.1	25.5	16.5 (min)	22.3	20.2	121
MLD 46	*A. africanus*	~3.0	38.4 (est)	30.1	19.8	-	-	120
Sts 14	*A. africanus*	2.0-2.6	30.8 (est)	22.6	14.2 (min)	-	-	118
StW 25	*A. africanus*	2.0-2.6	30.2	20.2	-	-	-	-
StW 99/100	*A. africanus? P. robustus ?*	2.0-2.6	39.1 (est)	27.1	19.1	34.6	26.1	113
StW 361	*A. africanus*	2.0-2.6	29.1	-	-	-	-	-
StW 392	*A. africanus*	2.0-2.6	31.5	19.2	-	-	-	-
StW 403	*A. africanus*	2.0-2.6	32.7 (est)	24.4	16.7	-	-	-

StW 479	*A. africanus*	2.0-2.6	32.7 (est)	23.5	17.4	-	-	-
StW 501	*A. africanus*	2.0-2.6	33.0	23.4	17.3	-	-	-
StW 522	*A. africanus*	2.0-2.6	30.4	20.6	15.2	-	-	124
StW 527	*A. africanus*	2.0-2.6	32.2	-	-	-	-	
StW 311	*Homo? P. robustus?*	2.2	35.7	26.9	19.3	-	-	-
U.W. 88-4,5,39	*A. sediba*	1.977	33.0 (est)	23.3	17.1	26.4	20.3	115
U.W. 88-51	*A. sediba*	1.977	32.7	22.4	16.6	-	-	-
SWT1/LB-2	*P. robustus*	1.8-2.25	34.4	25.9	17.7	-	-	-
SK 82	*P. robustus*	1.8-1.9	34.4	27.2	19.2	30.4	24.8	120
SK 97	*P. robustus*	1.8-1.9	37.2	26.2	19.6	35.3	23.3	118
SKW 19	*P. robustus*	1.8-1.9	30.2	-	-	-	-	-
SWT1/HR-2b	*P. robustus*	1.8-1.9	30.6	23.3	-	26.6	19.2	113
D4167	*Homo*	1.77	40.0	29.0	22.5	-	-	-
SK 3121	*P. robustus*	~1.4	28.6	19.1	16.0	-	-	-

Data from DeSilva et al., 2012; Pickering et al., 2012; Heaton et al., 2019; DeSilva & Grabowski, 2020; Pickering et al., 2021; Ward et al., 2023; Pickering et al., 2025 and measurements taken on original specimens.

Table 7. Patellae measurements (in mm)

Catalogue #	Taxon	Age	Height (PD)	Thickness (AP)	Width (ML)
KW 8182	Hominin	≥2.0	29.4	17.4	35.2
KW 11502	Hominin	≥2.0	-	13.5	25.4 (est)
U.W. 88-79,100	*A. sediba*	1.98	24.7	13.1	26.8
SKX 1084	Hominin	~1.4	-	13.3	30.2

Data from Susman, 1989; Marchi et al., 2017; DeSilva et al., 2018 and measurements taken on original specimens.

Table 8. Intermediate cuneiform measurements (in mm)

Catalogue #	Taxon	Age (Ma)	Minimum ML width (mm)	Maximum PD length (mm)	Maximum DP height (mm)
KW 6780	Hominin	≥2.0	11.4	12.6	13.2 (min)
StW 573	*A. prometheus*	3.67?	12.3	12.6	15.4
OH 8	*H. habilis? P. boisei?*	1.85	11.2	12.4	15.1

Data from DeSilva et al., 2019 and sources therein and measurements taken on original specimens.

Table 9. Navicular measurements (in mm)

Catalogue #	Taxon	Age (Ma)	Maximum ML width	Maximum DP height	PD thickness of tuberosity	DP height of tuberosity	Maximum length of talar facet	Maximum height of talar facet	Lateral PD thickness of body
KW 10699	Hominin	≥2.0	30.3	17.6	17.6	10.0	21.2	14.0	8.9
StW	*A.*	3.67	33.6	18.5	16.8	10.1	22.2	-	10.8

573	*prometheus*								
OH 8	*P. boisei? H. habilis ?*	1.85	31.4	18.6	15.5	9.2	23.8	15.8	10.1

1 Data from DeSilva et al., 2019 and sources therein and measurements taken on original
2 specimens.
3
4 Table 10. Calcanei measurements (in mm)

Catalogue #	Taxon	Age	Maximum length of preserved fragment	Anterior calcaneal length (from anterior most point of posterior talar facet to anteriormost point of cuboid facet)	Maximum height of distal body (near cuboid facet)	Minimum DP height of distal body (at base of posterior talar facet)	Maximum proximodistal length of posterior talar facet	Maximum mediolateral breadth of posterior talar facet	Maximum length of sustentaculum base	Dorsoplantar height of sustentaculum tali base	Calcaneocuboid joint angle
KW 12330	Hominin	≥2.0	38.1	18.1	20.2	17.4	21.6	16.0	19.4	9.6	103.7°
StW 352	*A. africanus*	2.0-2.6	50.1	19.0	19.1	16.0	22.0	14.5	19.4 (est)	9.8	-
KW	Homi	≥2.0	46.8	-	19.3	15.6	22.5	16.7	-	-	-

6302	nin				(est)			(est)			
U.W. 88-99	*A. sedibа*	1.98	56.9	13.2	23.1	19.4	19.8	17.3	19.5	9.1	98°
Omo-33-74-896	*H. habilis*? *P. boisei*?	2.36	69.4	17.5	27.4	19.5	28.4	19.4	21.4	9.3	99°
OH 8	*H. habilis*? *P. boisei*?	1.85	32.5	14.4	17.1	13.8	-	-	17.9	9.6	108°

1 Data from Prang, 2015; DeSilva et al., 2019 and sources therein, and Harper et al., 2022 and
2 measurements taken on original specimens.
3
4 Table 11. Third metatarsal measurements (in mm)

Catalogue #	Taxon	Age (Ma)	Base ML width (mm)	Base DP height (mm)
KW 6994	Hominin	≥2.0	12.4	17.1 (est)
StW 238	*A. africanus*	2.0-2.6	12.1	16.3
StW 387	*A. africanus*	2.0-2.6	10.9	16.7
StW 388	*A. africanus*	2.0-2.6	12.6	18.5
StW 435	*A. africanus*	2.0-2.6	13.3	20.1
StW 477	*A. africanus*	2.0-2.6	12.0	16.5
StW 496	*A. africanus*	2.0-2.6	10.9	16.8
KNM-ER 77071	*Homo?*	1.9	10.9	17.8
SKX 38529	*P. robustus?*	1.8-2.25	12.1	-
KNM-ER 1500	*P. boisei*	1.89	12.0	17.7
OH 8	*P. boisei?* *H. habilis?*	1.85	11.9	16.0
OH 43	*P. boisei?*	1.85	10.0	-

	H. habilis?			
KNM-ER 997	*P. boisei*?	1.85	10.1	16.2
Omo F.511-16	*Homo?*	1.7	14.6	20.7
KNM-ER 1823	*P. boisei*?	1.59	12.8	-
KNM-ER 803j	*H. erectus*	1.53	12.7	20.5
KNM-ER 101000	*P. boisei*	1.52	12.9	20.0
SKX 247	*P. robustus?*	~1.4	12.2	16.3

1 Data from DeSilva et al., 2019 and sources therein; Zipfel and Wunderlich, 2020; Hammond et
2 al., 2021; Mongle et al., 2025 and measurements taken on original specimens.
3

4 Table 12. First metatarsal measurements (in mm)

Catalogue #	Taxon	Age (Ma)	Length (mm)	Base ML width	Base DP height	Midshaft ML	Midshaft DP	Head ML width	Head DP height
KW 10829	Hominin	≥2.0	45.3	13.3	18.5	9.0	8.9	13.4	14.3
StW 573	*A. prometheus*	3.67	-	12.5	20.4	9.4	10.2	-	-
StW 595	*A. africanus*	2.0-2.6	45.7	13.0	18.1	7.6	8.5	15.0	12.2
StW 562	*A. africanus*	2.0-2.6	52.4	16.0	24.2	10.4	11.4	19.0	15.2
DNH 115	Hominin	~2.0	-	13.7	22.7	10.7	10.5	-	-
SK 5017	*P. robustus*	1.8-2.25	43.5	16.0	21.7	10.4	11.6	17.7	16.5
SK 1813	*P. robustus*	1.4-2.25	41.4	13.3 (est)	17.4 (est)	10.3	10.6	13.3	14.6

OH 8	*P. boisei? H. habilis ?*	1.85	43.9 (est)	15.9	21.3	10.6	10.5	-	-

Data from Susman and Brain, 1988; Susman and de Ruiter, 2004; DeSilva et al., 2019 and sources therein; Zipfel and Wunderlich, 2020; Orr et al., 2026 and measurements taken on original specimens.

Table 13. Proximal pedal phalanges measurements (in mm)

Catalogue #	Element	Species	Age	Length	Base ML	Base DP	Midshaft ML	Midshaft DP	Head ML	Head DP	Articular angle
KW 11666	PP	Hominin	≥2.0	19.4 (min)	9.9	6.9	6.2	5.2	8.1 (min)	5.2 (min)	97
KW 12276	PP5	Hominin	≥2.0	15.6	7.2	5.4	4.0	2.9	5.6	3.6	103
StW 355	PP2?	*A. africanus*	2.0-2.6	24.6	9.1	7.8	5.9	5.0	7.1	4.5	96
DNH 117	PP	Hominin	~2.0	24.1	10.5	9.1	6.6	5.1	8.2	4.9	105
SKX 16699	PP3, 4, or 5	*Homo?*	1.8-2.25	20.3	8.9	8.6	4.7	4.5	6.9	4.8	110
KNM-ER 803r	PP	*H. erectus*	1.53	-	-	-	6.9	6.1	9.0	6.3	-
KNM-ER 101000	PP	*P. boisei*	1.52	25.0	9.9	9.6	5.6	5.1	8.4	5.4	107

Data from Trinkaus & Patel, 2016; DeSilva et al., 2019; Zipfel and Wunderlich, 2020; Mongle et al., 2025; Orr et al., 2026 and measurements taken on original specimens.

Table 14. Distal hallucal phalanges measurements (in mm)

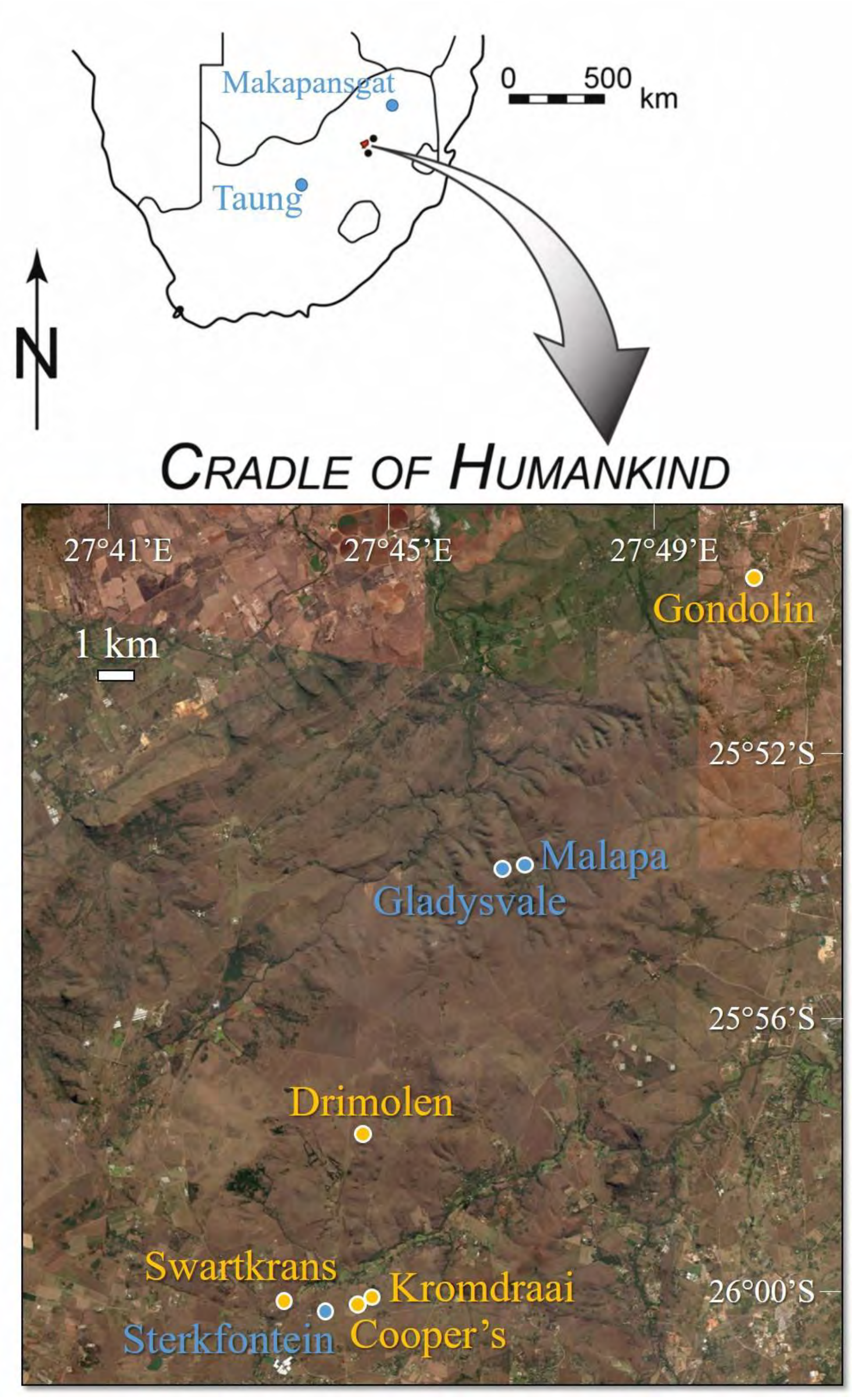
Catalogue #	Taxon	Age (Ma)	Maximum length	Base ML	Base DP	Midshaft ML	Midshaft DP	Head ML	Head DP	Transverse angle	Axial torsion
KW 11099	Hominin	≥2.0	16.8	14.0	7.6	8.5	5.3	10.0	4.4	1.5	5.0
StW 617	*A. africanus*	2.0-2.6	15.4	13.8	6.4	9.6	4.4	9.5	5.1	3.5	-2.0
OH 10	*H. habilis? P. boisei?*	1.8	17.5	18.3	6.7	9.3	4.6	12.2	3.8	2.0	13.0
TM1517k	*P. robustus*	1.4-1.8	15.3	9.8 (min)	4.2	7.4	5.3	9.2	4.6	2.0	15.0

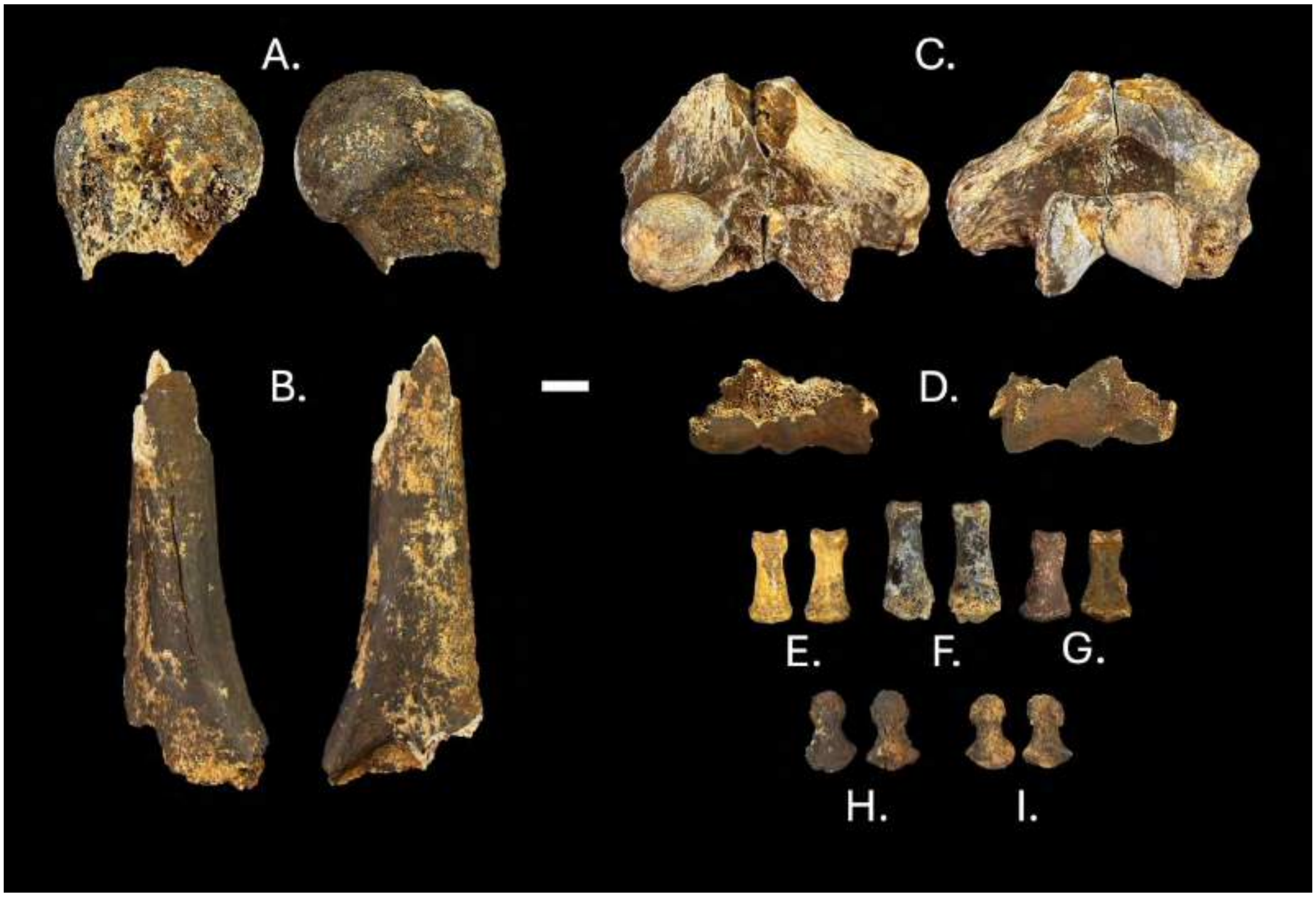
1 Data from Day, 1986; Day and Thornton, 1986; DeSilva et al., 2019; Zipfel and Wunderlich,
2 2020 and measurement taken on original specimens.
3
4 Table 15. Body mass estimates for hominin postcrania in Unit P, Kromdraai

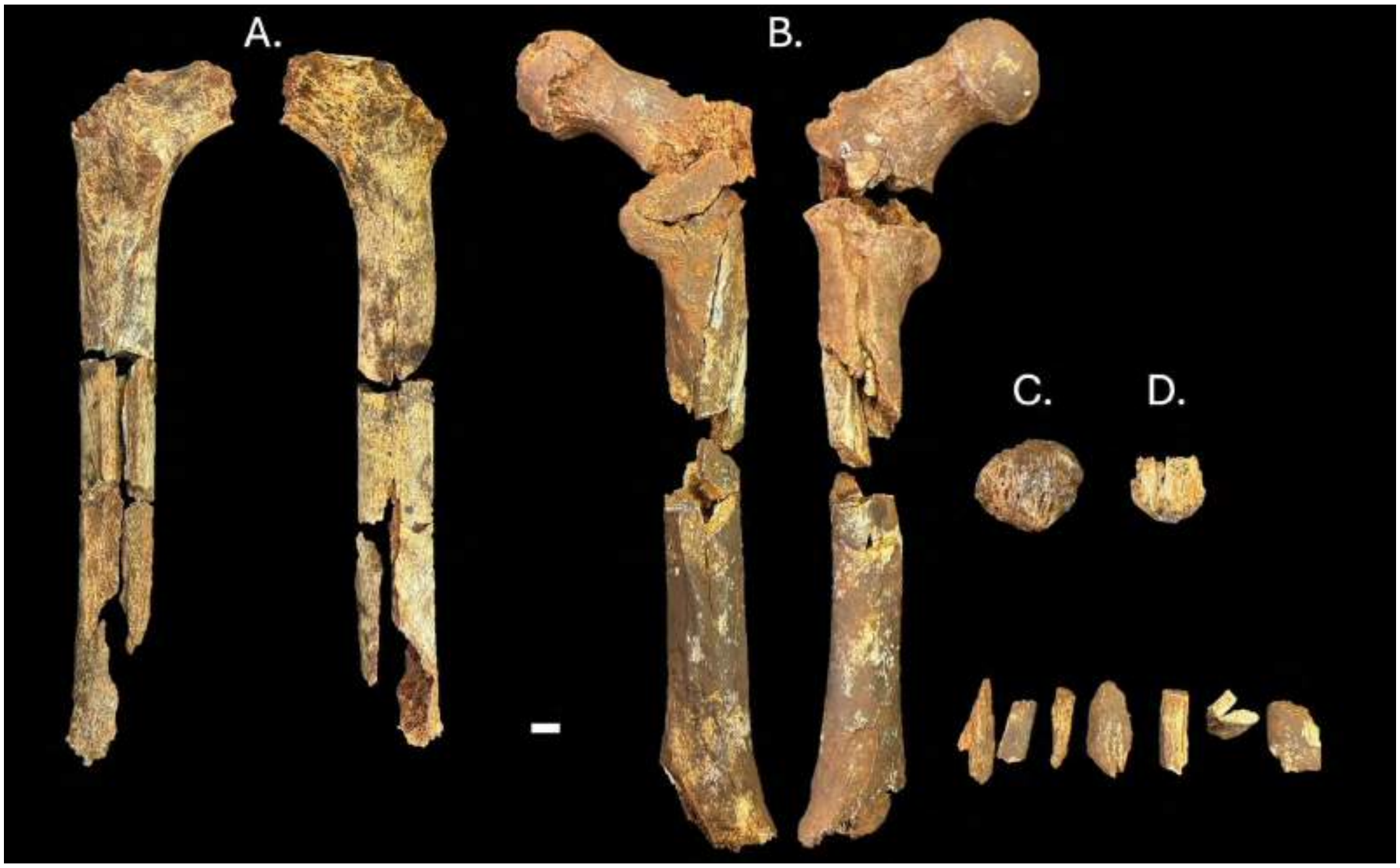
Catalogue #	Element	Measurement used to calculate body mass	Body mass estimate	Reference	Notes
KW 9620	Proximal humerus	Humeral head SI	27.8 kg	Burgess et al., 2018	Chimpanzee reference used following Ruff et al., 2020
KW 8246	Distal humerus	Articular width ML	66.4 kg	Burgess et al., 2018	Chimpanzee reference used following Ruff et al., 2020
KW 9970	Distal	Articular	30.1 kg	Burgess et al.,	Chimpanzee

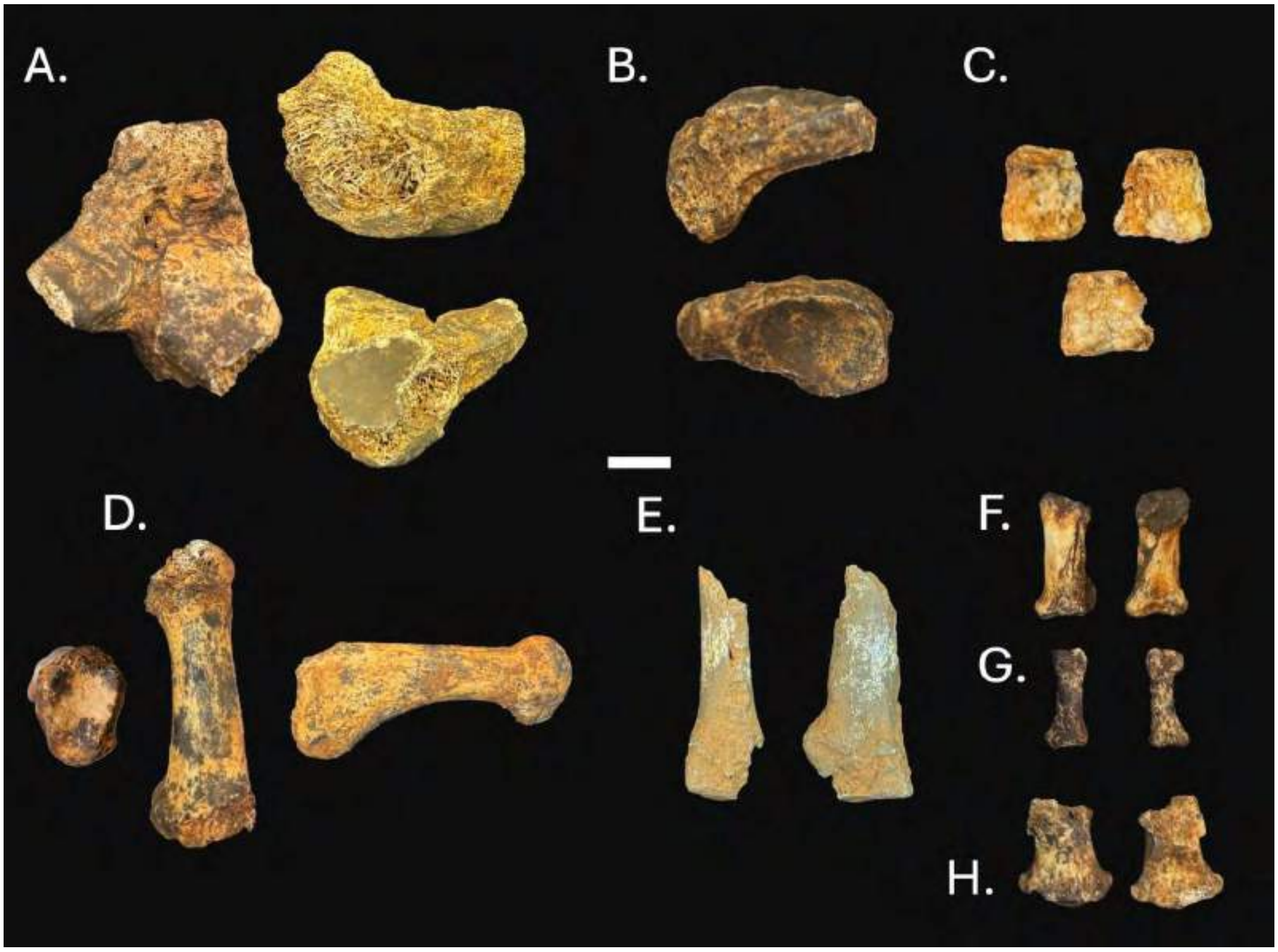
	humerus	width ML		2018	reference used following Ruff et al., 2020
KW 9950	Proximal femur	Femoral head diameter	32.9 kg	Grabowski et al., 2015	Equations in Ruff & Wood (2023) and Ruff et al., 2020 yield a higher BM estimate of 43.6 kg
KW 6302	Calcaneus	Talar body width	33.8-35.9 kg	Harper et al., 2022	Equation from McHenry (1992)
KW 10827	First metatarsal	Dorsoplantar height of proximal articular surface	28.6 kg	De Groote & Humphrey, 2011	Applying this method on the StW 573 Mt1 yields a BM estimate of 35.3 kg, similar to the 33.2 kg estimate from the FHD (Crompton et al., 2022)

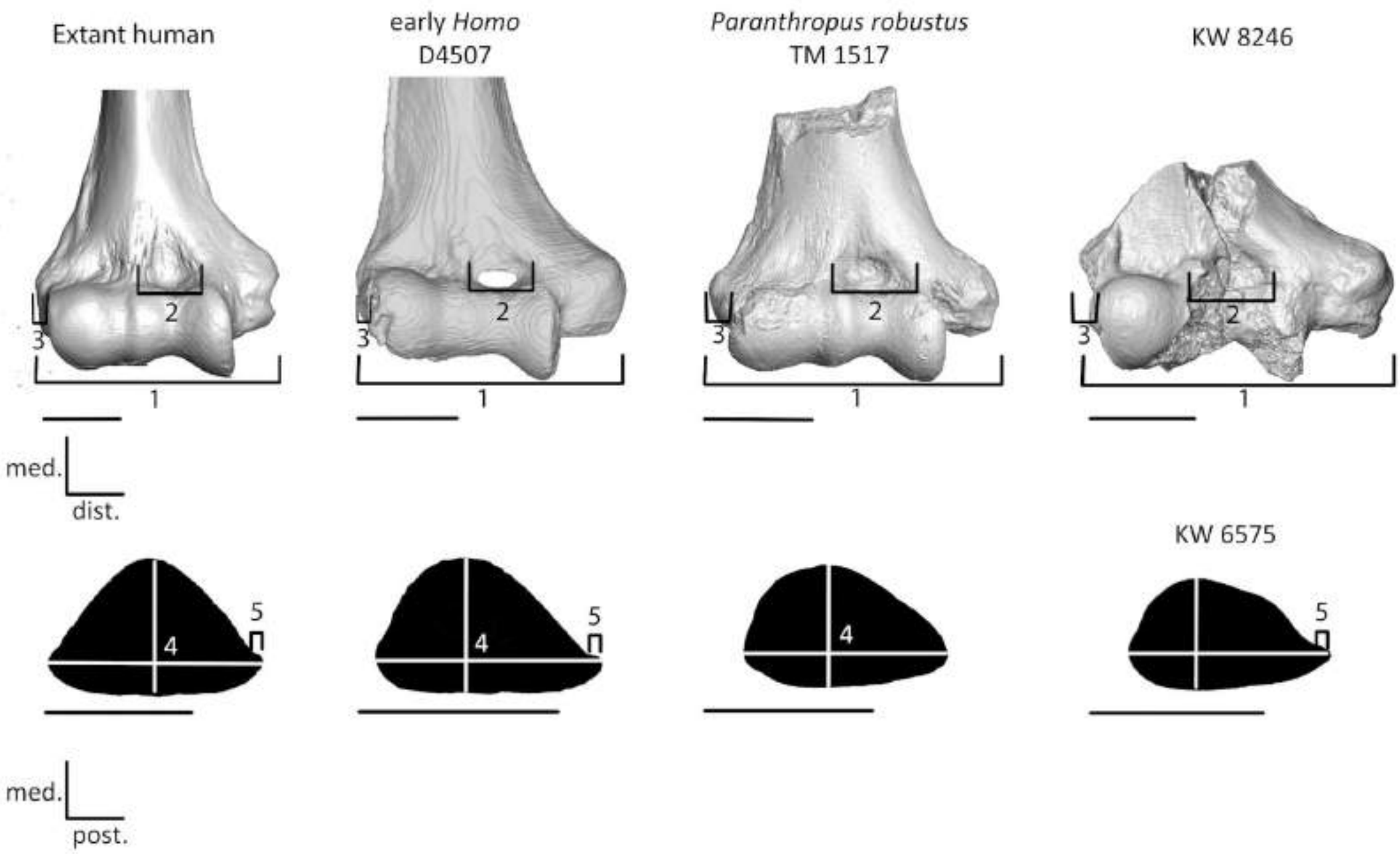
1

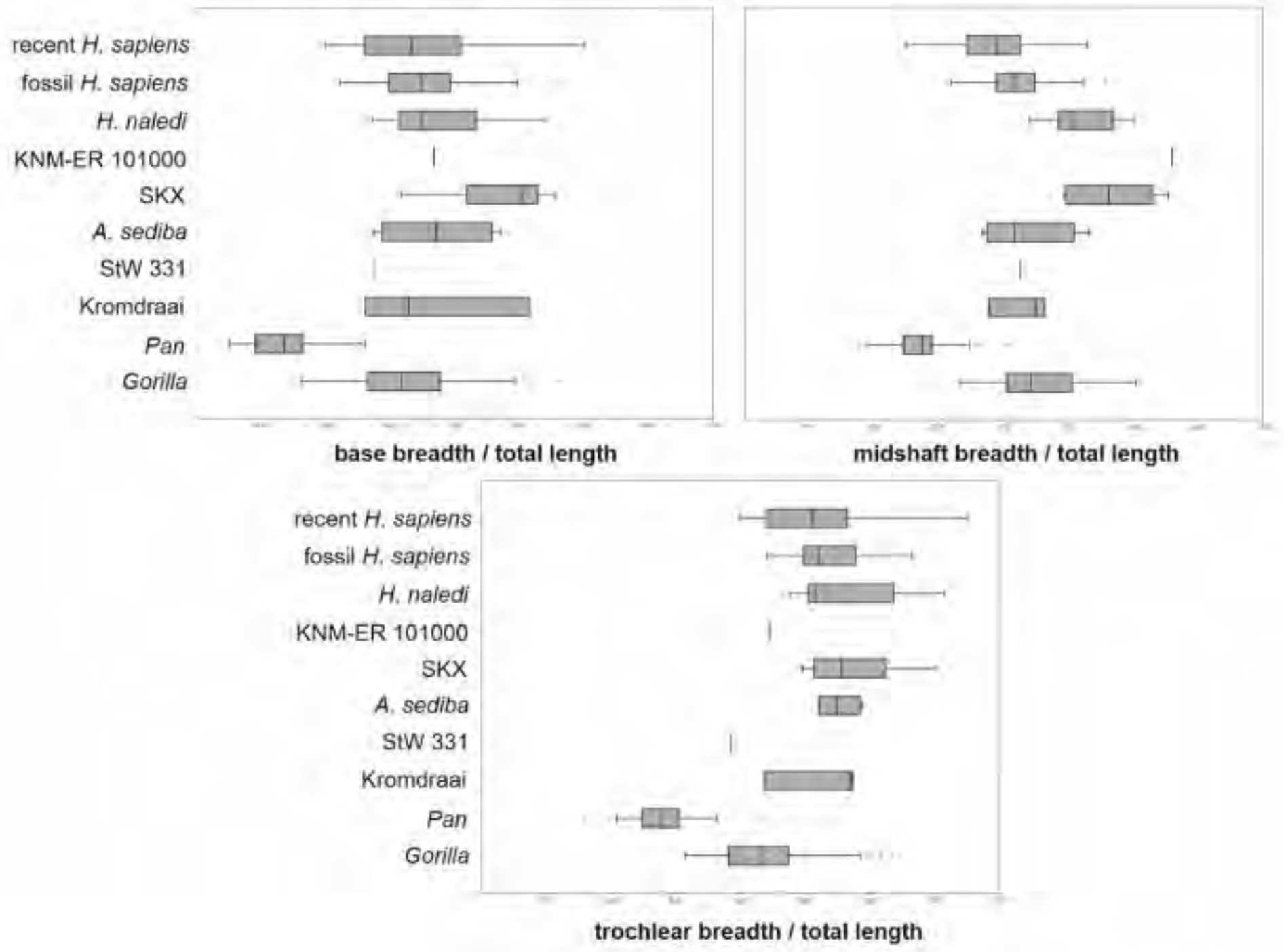

Makapansgat
Taung
0 500 km
N
CRADLE OF HUMANKIND
27°41'E
27°45'E
27°49'E
1 km
Gondolin
25°52'S
Malapa
Gladysvale
25°56'S
Drimolen
Swartkrans
Kromdraai
Sterkfontein
Cooper's
26°00'S

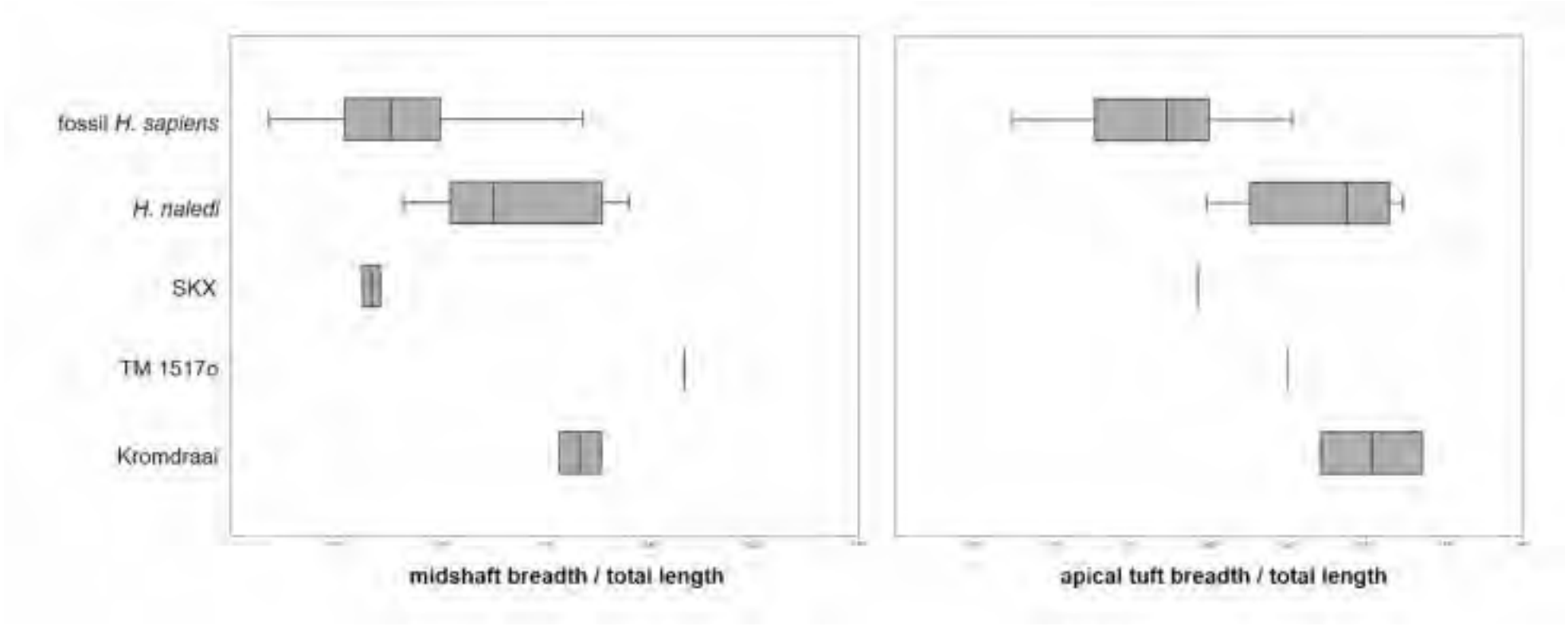

A.
B.
C.
D.
E.
F.
G.
H.
I.

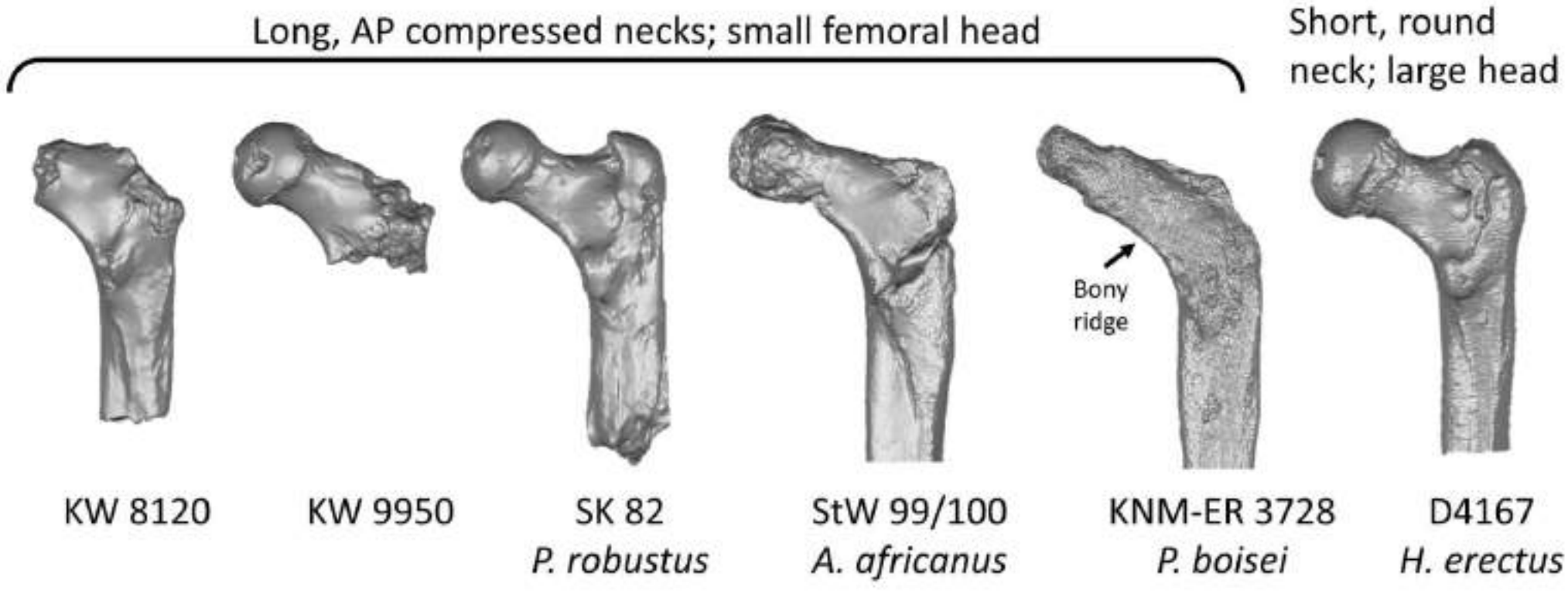

A.
B.
C.
D.

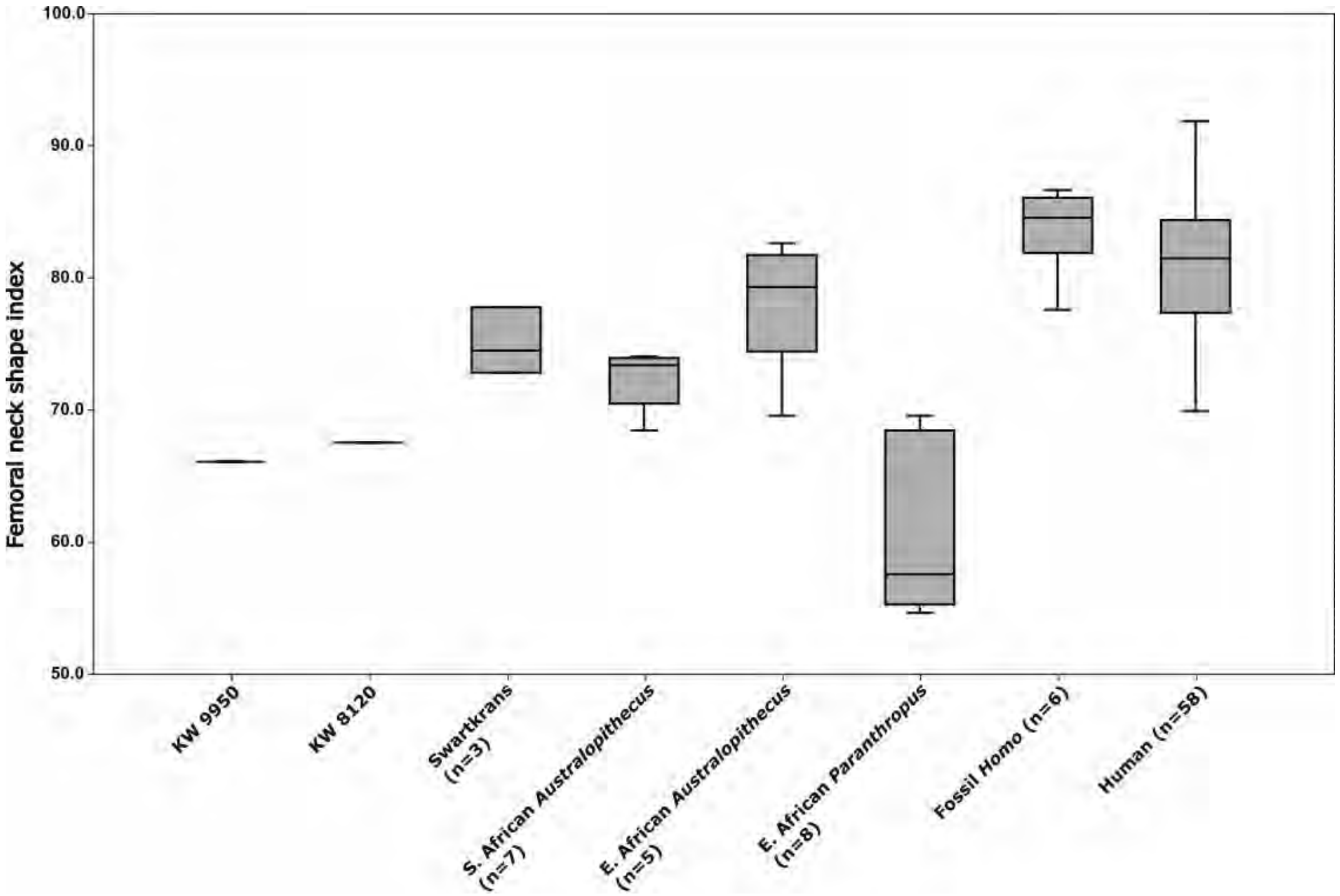

A.
B.
C.
D.
E.
F.
G.
H.


Extant human
early *Homo*
D4507
Paranthropus robustus
TM 1517
KW 8246
1
2
3
4
5
med.
dist.
post.
KW 6575

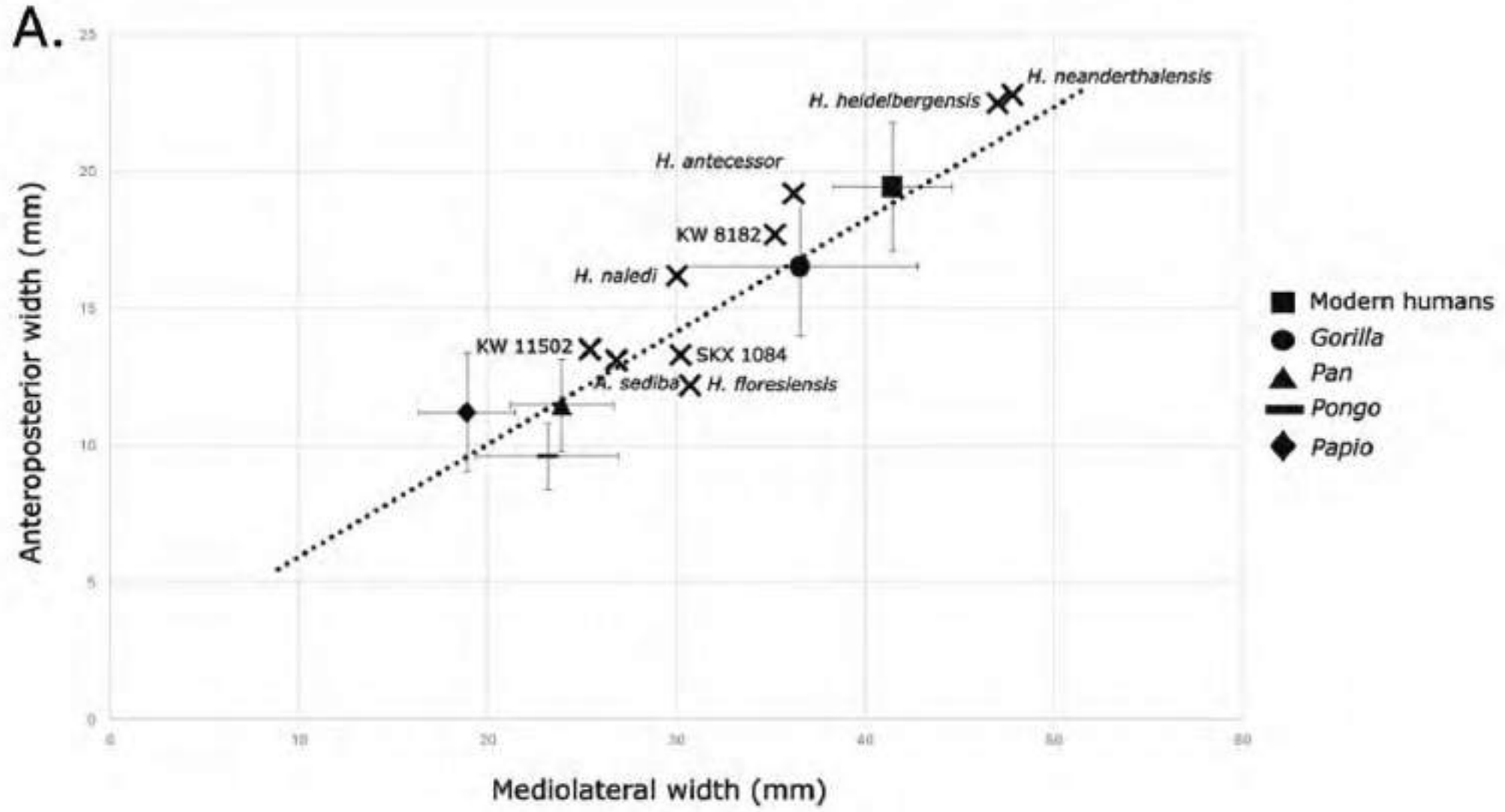

recent H. sapiens
fossil H. sapiens
H. naledi
KNM-ER 101000
SKX
A. sediba
StW 331
Kromdraai
Pan
Gorilla
base breadth / total length
midshaft breadth / total length
trochlear breadth / total length


fossil H. sapiens
H. naledi
SKX
TM 1517c
Kromdraai
midshaft breadth / total length
apical tuft breadth / total length

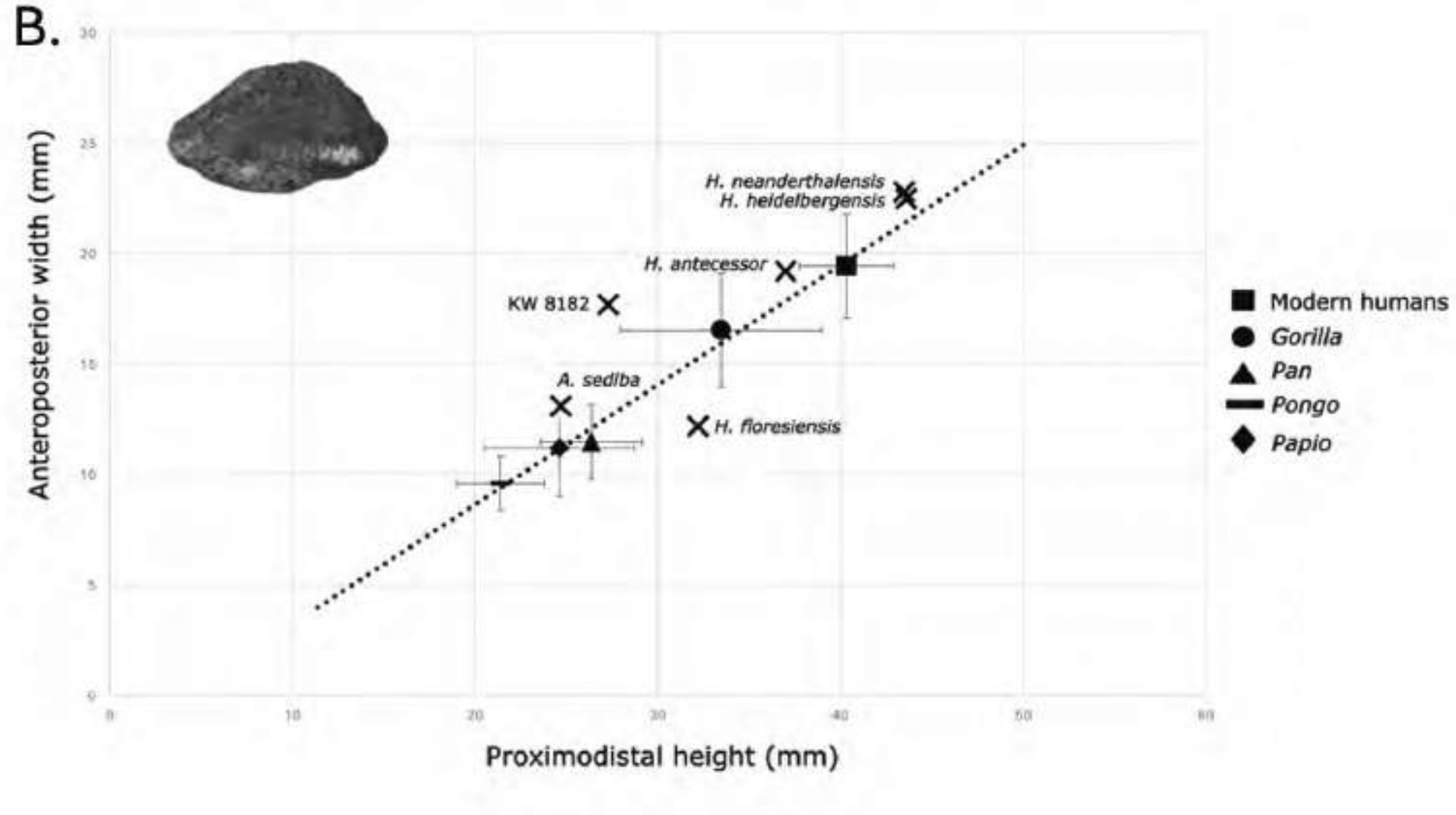

Long, AP compressed necks; small femoral head
Short, round neck; large head
Bony ridge
KW 8120
KW 9950
SK 82
P. robustus
StW 99/100
A. africanus
KNM-ER 3728
P. boisei
D4167
H. erectus

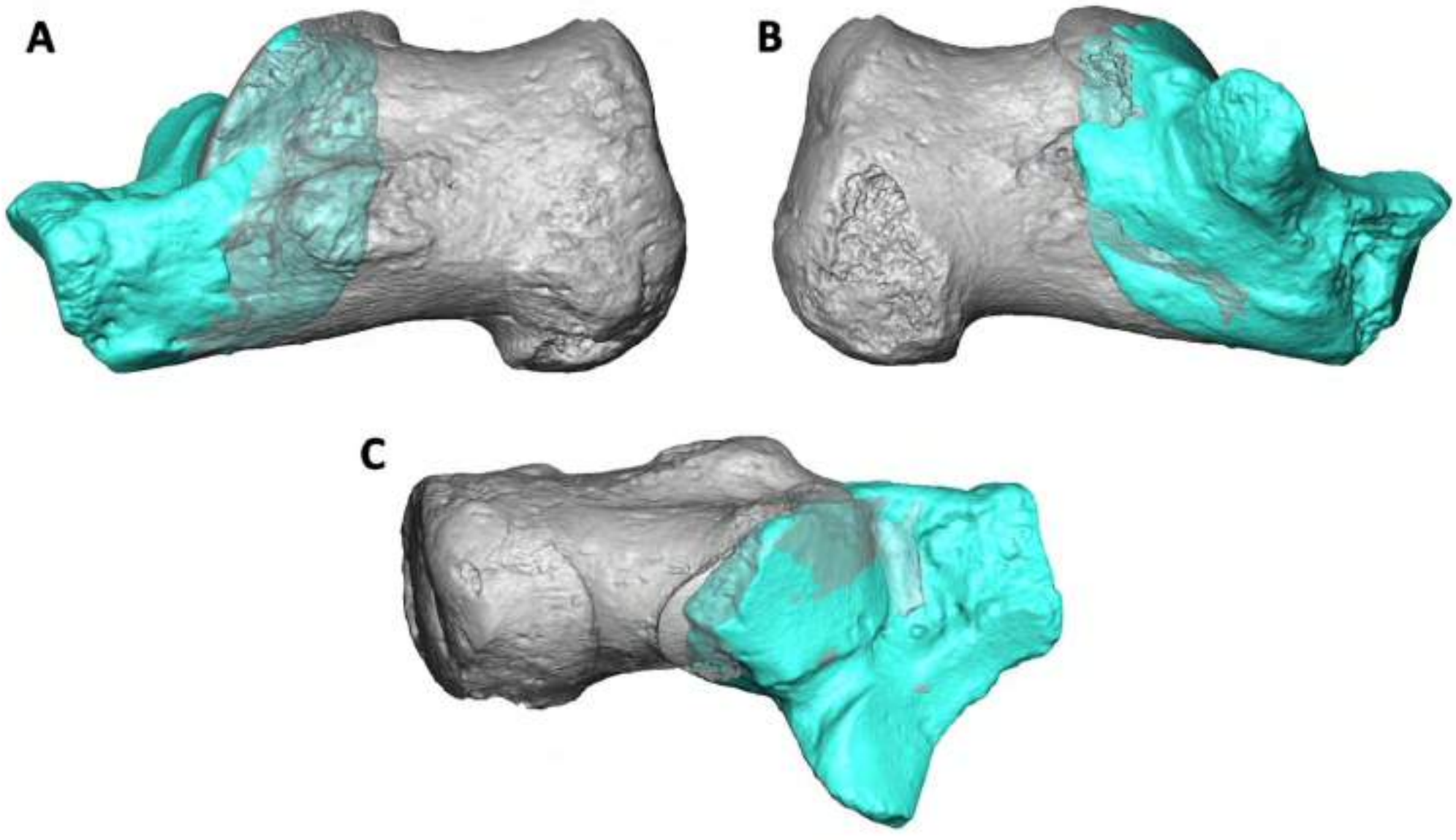

Femoral neck shape index
100.0
90.0
80.0
70.0
60.0
50.0
KW 9950
KW 8120
Swartkrans (n=3)
S. African Australopithecus (n=7)
E. African Australopithecus (n=5)
E. African Paranthropus (n=8)
Fossil Homo (n=6)
Human (n=58)

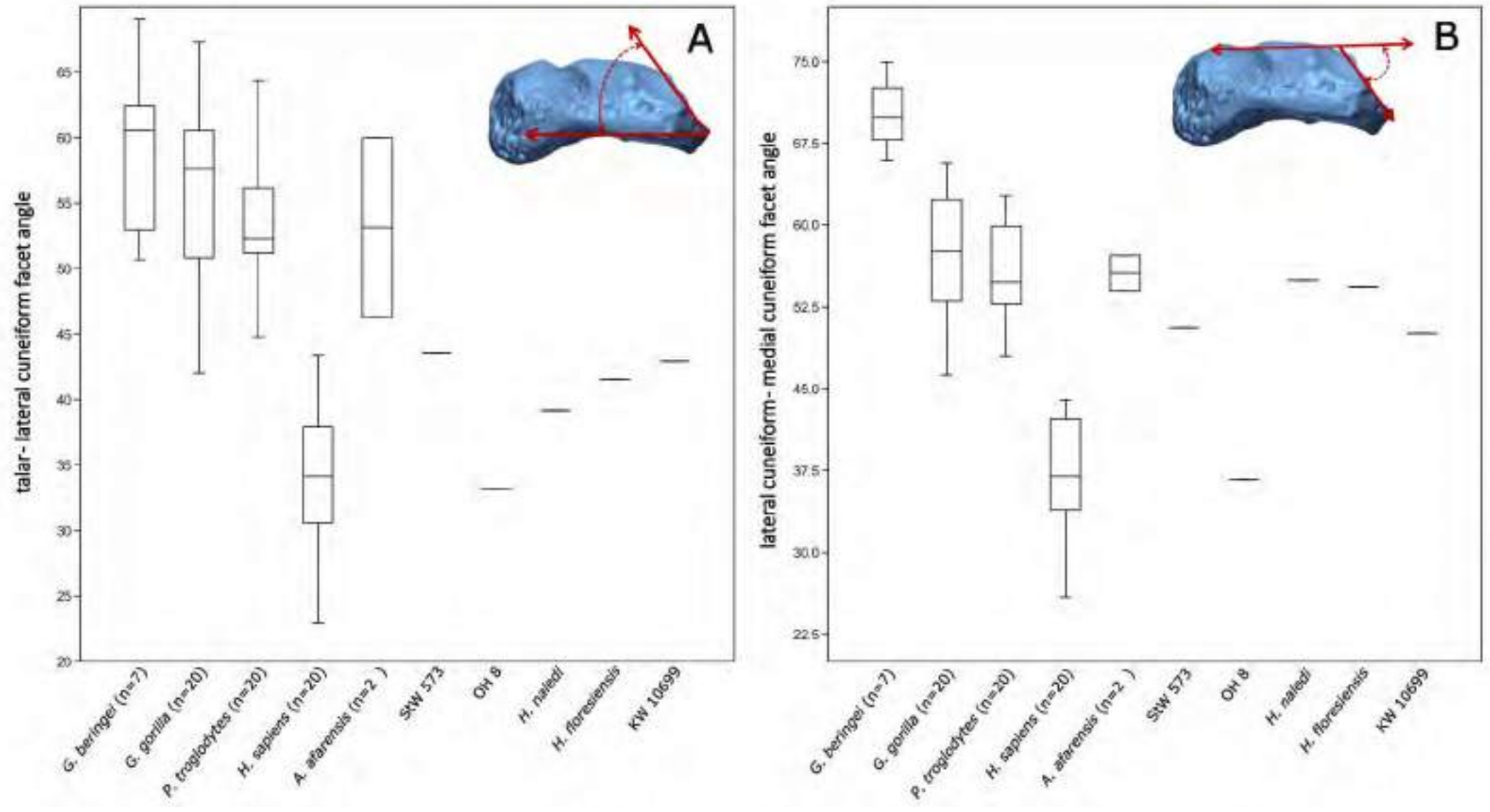
A.

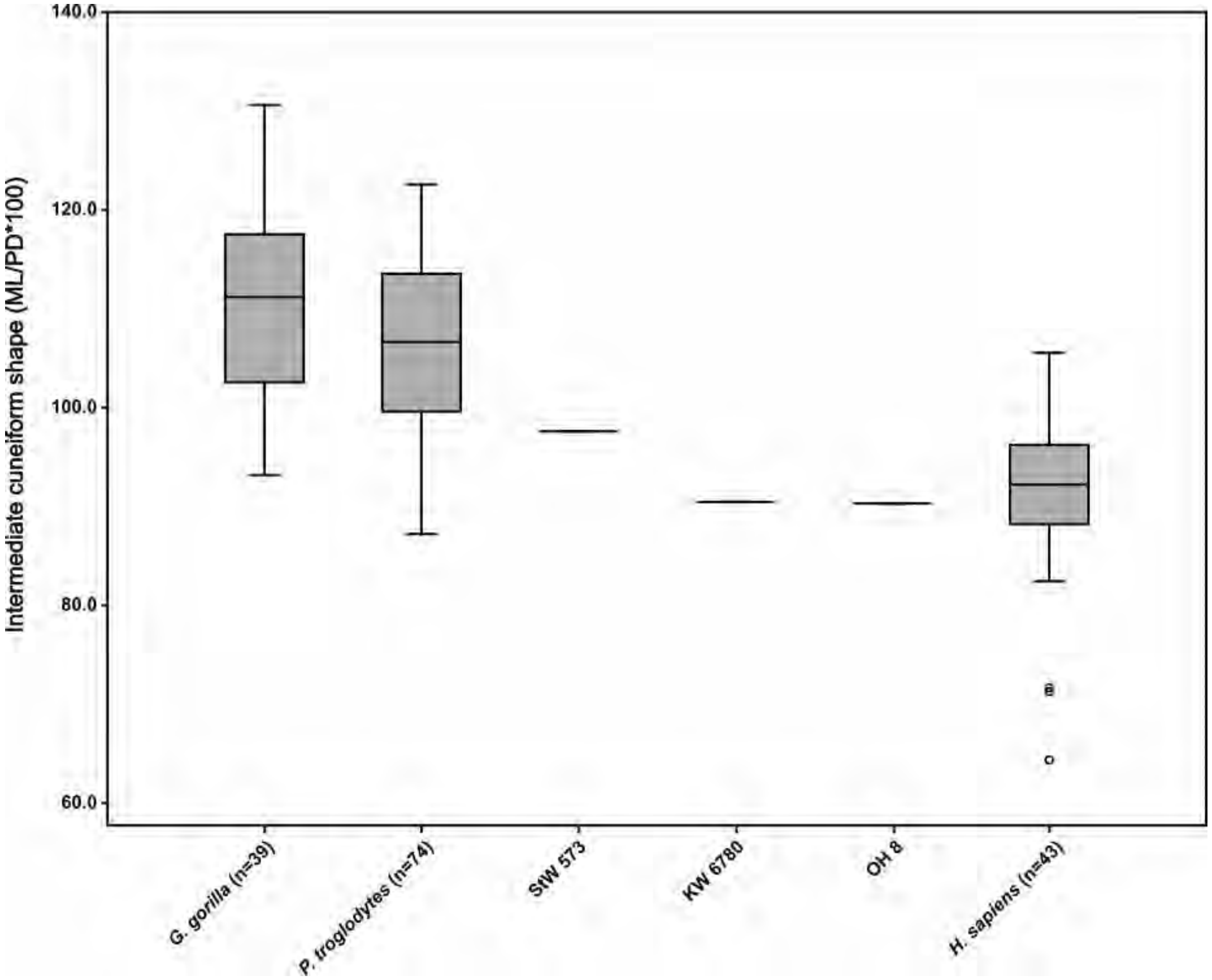

Anteroposterior width (mm)
Mediolateral width (mm)
H. neanderthalensis
H. heidelbergensis
H. antecessor
KW 8182
H. naledi
KW 11502
SKX 1084
A. sediba
H. floresiensis
Modern humans
Gorilla
Pan
Pongo
Papio

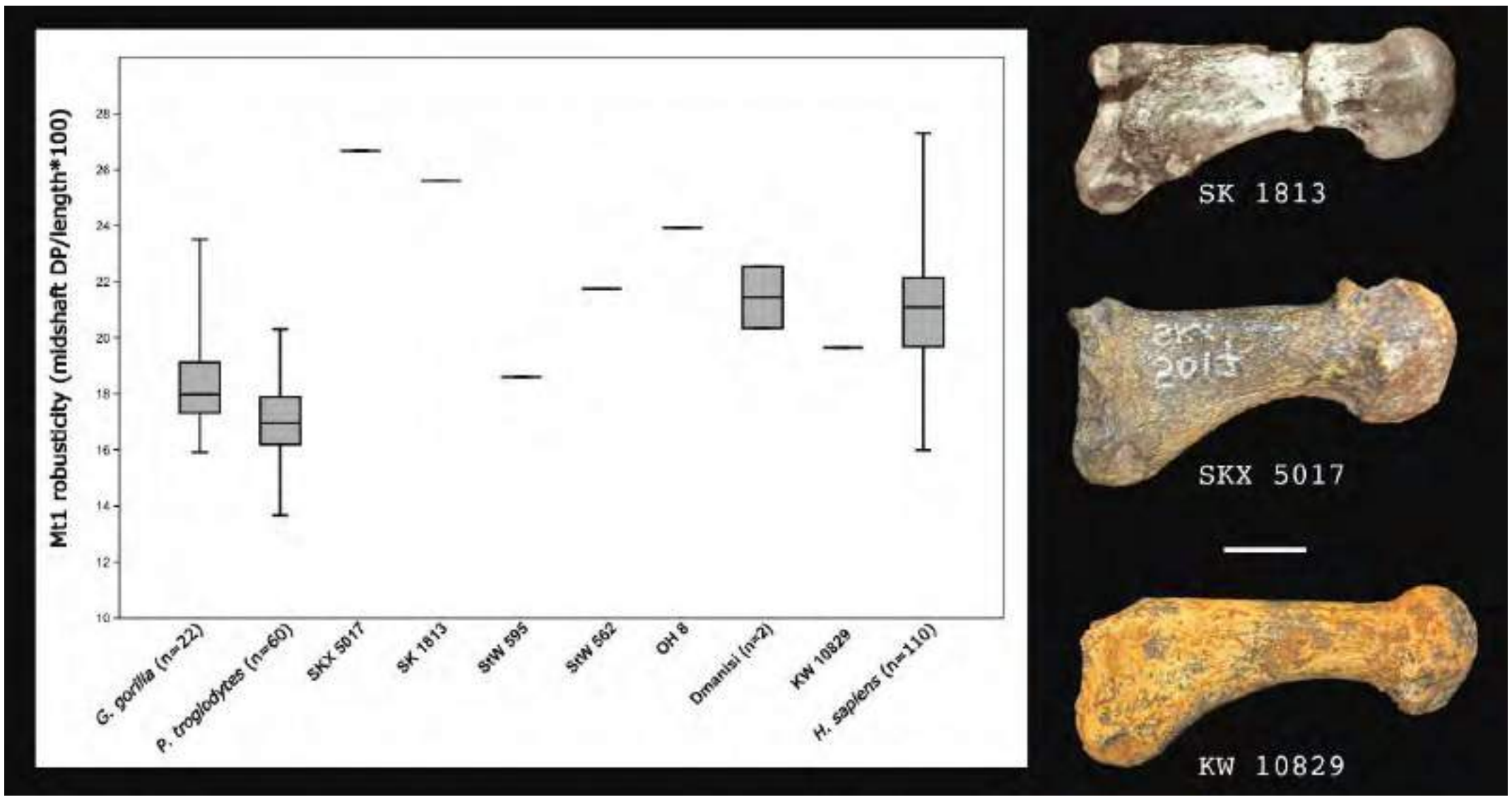
B.

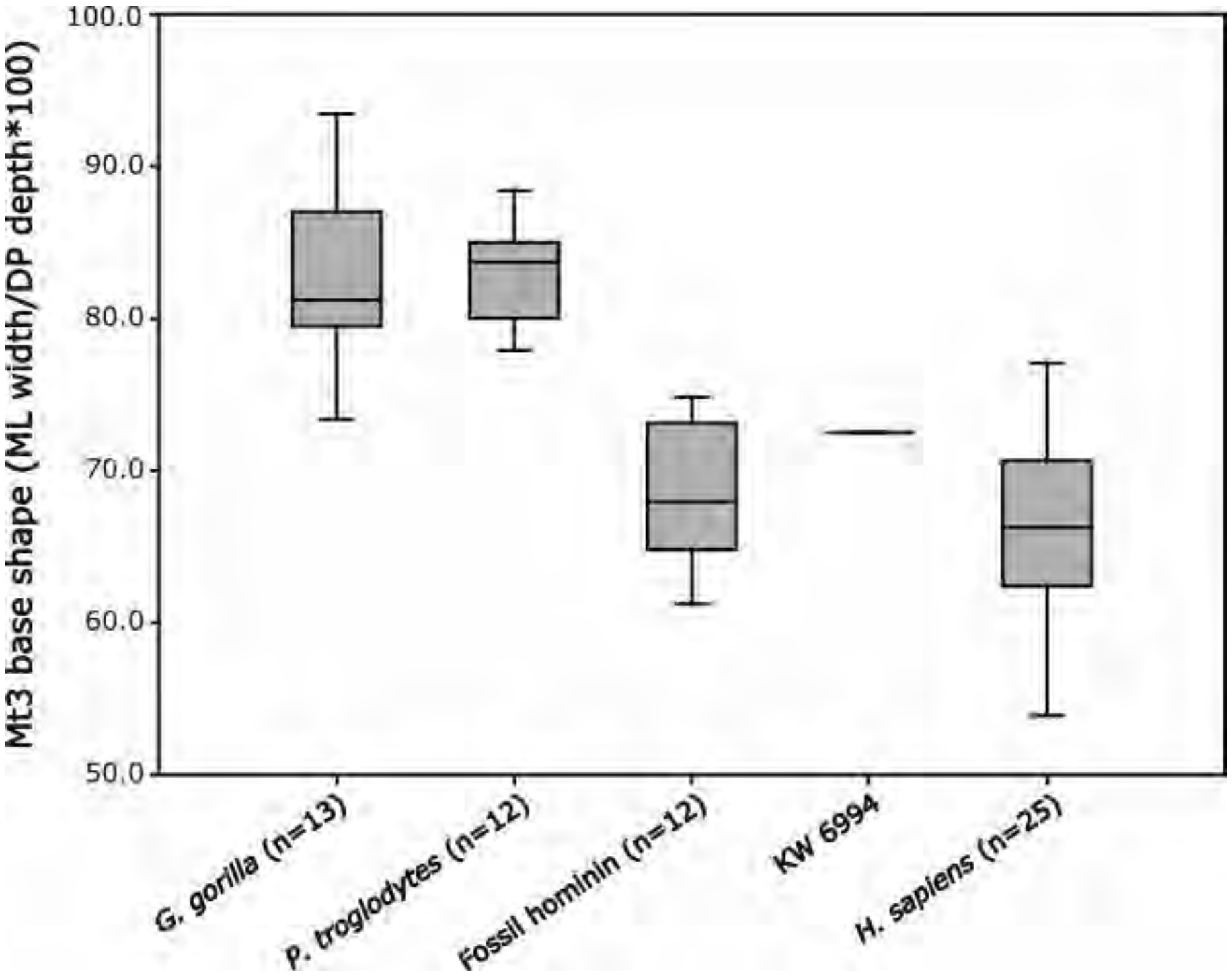

Anteroposterior width (mm)
Proximodistal height (mm)
H. neanderthalensis
H. heidelbergensis
H. antecessor
KW 8182
A. sediba
H. floresiensis
Modern humans
Gorilla
Pan
Pongo
Papio

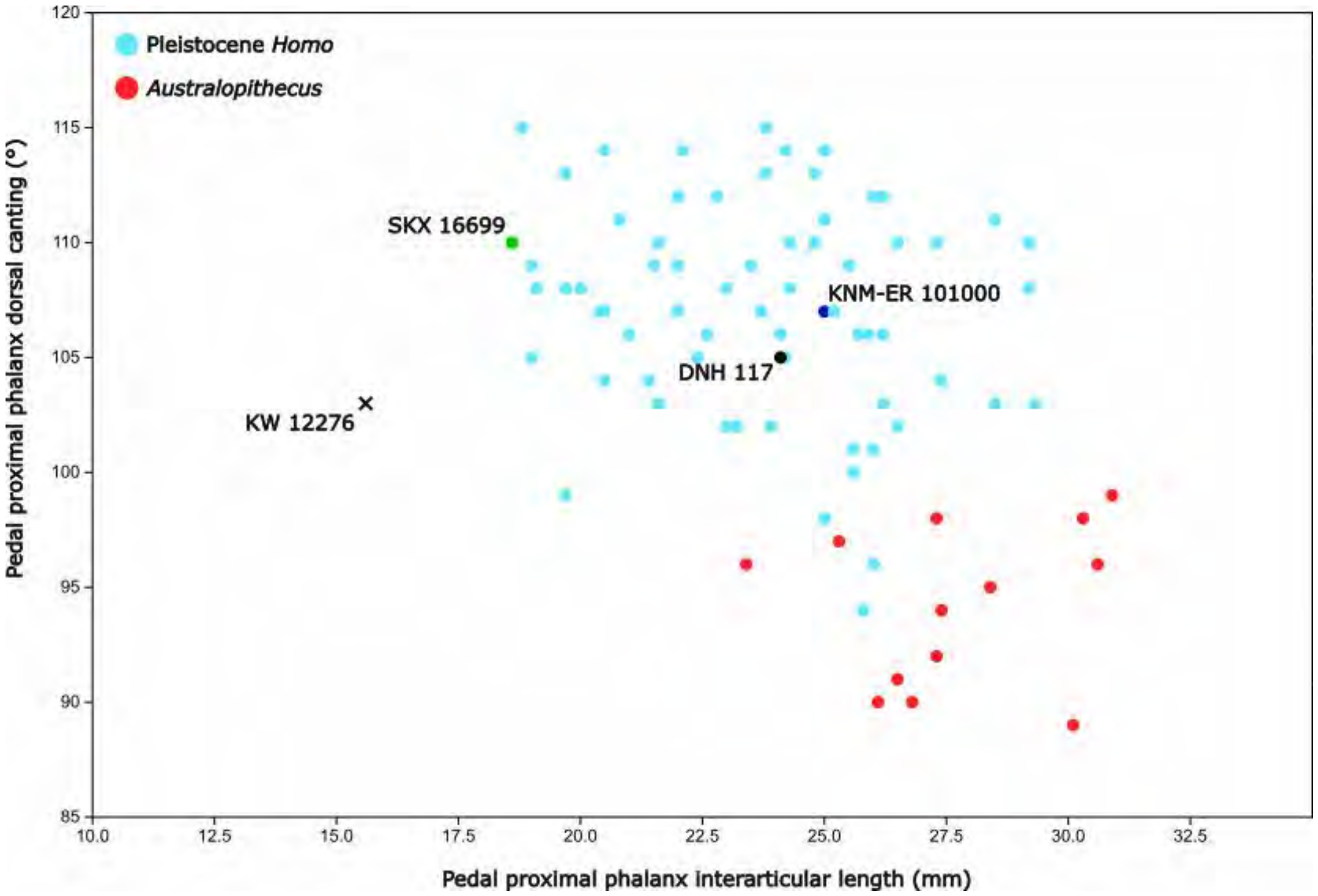

A
B
C


A
talar- lateral cuneiform facet angle
65
60
55
50
45
40
35
30
25
20
G. beringei (n=7)
G. gorilla (n=20)
P. troglodytes (n=20)
H. sapiens (n=20)
A. afarensis (n=2)
StW 573
OH 8
H. naledi
H. floresiensis
KW 10699
B
lateral cuneiform- medial cuneiform facet angle
75.0
67.5
60.0
52.5
45.0
37.5
30.0
22.5
G. beringei (n=7)
G. gorilla (n=20)
P. troglodytes (n=20)
H. sapiens (n=20)
A. afarensis (n=2)
StW 573
OH 8
H. naledi
H. floresiensis
KW 10699


Intermediate cuneiform shape (ML/PD*100)
140.0
120.0
100.0
80.0
60.0
G. gorilla (n=39)
P. troglodytes (n=74)
StW 573
KW 6780
OH 8
H. sapiens (n=43)

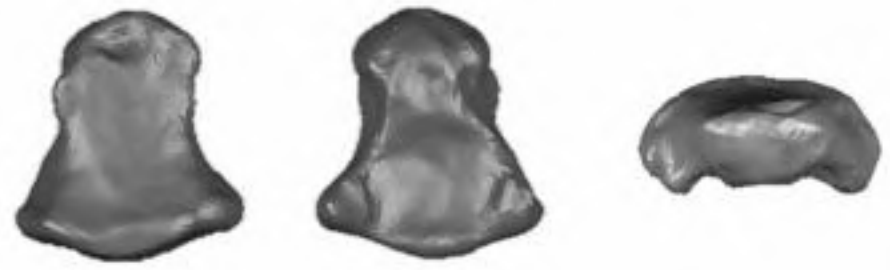

Mt1 robusticity (midshaft DP/length*100)
28
26
24
22
20
18
16
14
12
10
G. gorilla (n=22)
P. troglodytes (n=60)
SKX 5017
SK 1813
StW 595
StW 562
OH 8
Omanisi (n=2)
KW 10829
H. sapiens (n=110)
SK 1813
SKX 5017
KW 10829


Mt3 base shape (ML width/DP depth*100)
100.0
90.0
80.0
70.0
60.0
50.0
G. gorilla (n=13)
P. troglodytes (n=12)
Fossil hominin (n=12)
KW 6994
H. sapiens (n=25)


Pleistocene Homo
Australopithecus
SKX 16699
KNM-ER 101000
DNH 117
KW 12276
Pedal proximal phalanx dorsal canting (°)
120
115
110
105
100
95
90
85
10.0
12.5
15.0
17.5
20.0
22.5
25.0
27.5
30.0
32.5
Pedal proximal phalanx interarticular length (mm)



KW 11099



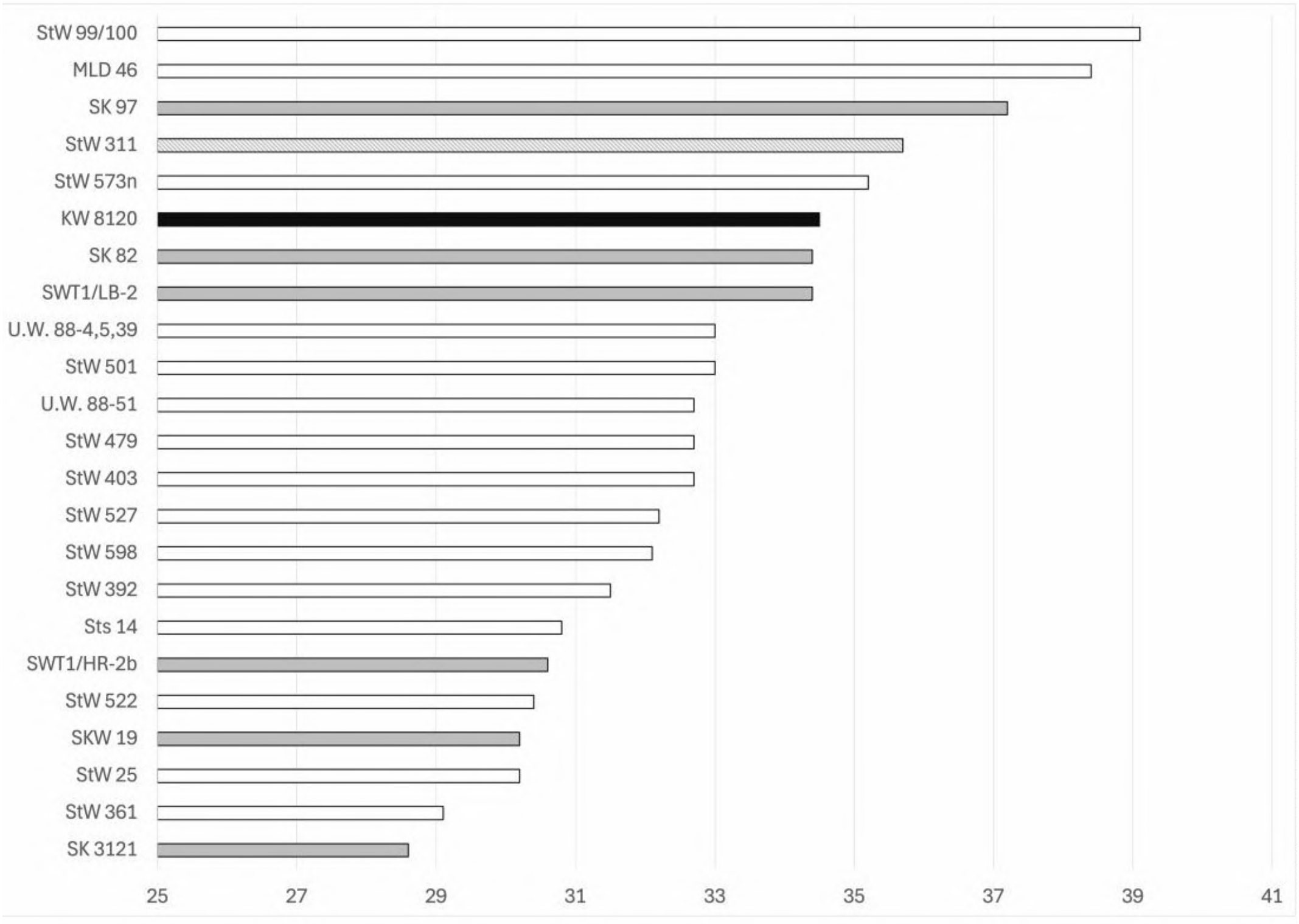
StW 617– *A. africanus*



TM 1517k– *P. robustus*



OH 10– *H. habilis*


StW 99/100
MLD 46
SK 97
StW 311
StW 573n
KW 8120
SK 82
SWT1/LB-2
U.W. 88-4,5,39
StW 501
U.W. 88-51
StW 479
StW 403
StW 527
StW 598
StW 392
Sts 14
SWT1/HR-2b
StW 522
SKW 19
StW 25
StW 361
SK 3121
25
27
29
31
33
35
37
39
41